

## Probing power spectrum enhancement at small scales with SKA

HOUI ZHU <sup>1,2</sup> BIN YUE <sup>1</sup> YIDONG XU <sup>1</sup> XUELEI CHEN <sup>1,2</sup> AND ZHIQI HUANG <sup>3,4</sup>

<sup>1</sup>*State Key Laboratory of Radio Astronomy and Technology, National Astronomical Observatories, Chinese Academy of Sciences, 20A Datun Road, Chaoyang District, Beijing 100101, China*

<sup>2</sup>*School of Astronomy and Space Science, University of Chinese Academy of Sciences, No.1 Yanqihu East Rd, Huairou District, Beijing 101408, China*

<sup>3</sup>*School of Physics and Astronomy, Sun Yat-sen University, 2 Daxue Road, Tangjia, Zhuhai 519082, China*

<sup>4</sup>*CSST Science Center for the Guangdong-Hongkong-Macau Greater Bay Area, Sun Yat-sen University, Zhuhai 519082, China*

### ABSTRACT

The reionization process is driven by ionizing photons from dwarf galaxies in halos with virial temperature  $T_{\text{vir}} \gtrsim 10^4$  K, while minihalos whose  $T_{\text{vir}} \lesssim 10^4$  K consume ionizing photons and have negative contributions to reionization. Since ionizing sources and minihalos have different clustering characteristics, not only the reionization history, but also the morphology of the ionization field, is sensitive to the small-scale power spectrum. If the power spectrum at small scales is enhanced compared with the standard six-parameter  $\Lambda$ CDM model, then both the sources and sinks of ionizing photons would be boosted and the net impact depends on the competition between them. Therefore, the 21 cm signal that can probe the morphology of the ionization field will be a useful tool for detecting the small-scale power spectrum. Using the power spectrum proposed by Cielo et al. (2025) (C25) as a demonstration, we investigate the influence of small-scale power spectrum enhancement on the ionization field and the 21 cm signal. We find that for the C25 model, even under the constraints of observed UV luminosity functions for high- $z$  galaxies and reionization history, the 21 cm power spectrum and the bubble size distribution could be still significantly different from the regular  $\Lambda$ CDM model. The upcoming SKA-low AA\* telescope, and a further imaging telescope, have the potential to detect the small-scale power spectrum more deeply.

*Keywords:* Cosmology (343) — Reionization (1383) — H I line emission (690) — High-redshift galaxies (734) — Intergalactic medium (813) — radio interferometry (1346)

### 1. INTRODUCTION

The matter power spectrum at the smallest scales remains an open question in cosmology. Primordial fluctuations are produced during the inflation stage, their evolution depends on the properties of dark matter particles. Although the Lambda cold dark matter ( $\Lambda$ CDM) model, with density fluctuations extending down to the damping scales of cold dark matter (CDM) particles (the mass scale of the CDM fluctuations damping is  $\sim$ an Earth mass, see J. Diemand et al. 2005; J. Wang et al. 2020), has been used as the standard model in research (e.g. Planck Collaboration et al. 2020), other models give rather different fluctuations levels at small scales. For example, in the Warm Dark Matter (WDM) model

(P. Bode et al. 2001; M. Viel et al. 2005; R. E. Smith & K. Markovic 2011) or Fuzzy Dark Matter (FDM) model (D. Jones et al. 2021; Y. Gong et al. 2023), the power spectrum starts to damp at scales much larger than the CDM damping scale. Therefore the formation of small dark matter halos are heavily suppressed. This has significant influence on the high- $z$  galaxy population (Y. Gong et al. 2023) and the reionization process (R. Barkana et al. 2001; B. Yue & X. Chen 2012). Alternatively, there are also models with small-scale fluctuations enhanced significantly compared to the regular  $\Lambda$ CDM model (e.g. M. Braglia et al. 2020; D. Inman & K. Kohri 2023; M. Cielo et al. 2025; E. O. Nadler et al. 2025). The enhancement of the small-scale power spectrum could be an interpretation of the observed galaxies excess at high redshifts (S. Hirano & N. Yoshida 2024; M. V. Tkachev et al. 2024).

The abundance of the high- $z$  galaxy population, i.e. the UV luminosity functions (UV LFs), can be a probe

of small-scale power spectrum and dark matter properties (P. Dayal et al. 2017; A. Rudakovskiy et al. 2021; B. Liu et al. 2024; P. Dayal & S. K. Giri 2024; S. Liu et al. 2025). The James Webb Space Telescope (JWST) has detected many faint high- $z$  galaxies (e.g. R. P. Naidu et al. 2022; S. L. Finkelstein et al. 2022; M. Castellano et al. 2022; L. D. Bradley et al. 2023; H. Atek et al. 2023), however, they are actually classified as the rare and brightest ones among the high- $z$  galaxy population. Their host dark matter halos are  $\gtrsim 10^{10} M_{\odot}$  (R. Endres et al. 2020). Observing power spectrum at smaller scales is rather challenging, because small-scale structures generally host very faint galaxies or even do not host any luminous objects. The Ly $\alpha$  forest is considered as the most powerful tool for probing subgalactic-scale power spectrum, and it has detected structures down the  $k \sim 1 - 10 \text{ Mpc}^{-1}$  (M. Viel et al. 2005; S. Chabanier et al. 2019), WDM particles mass up to  $\sim 3 - 5 \text{ keV}$  (M. Viel et al. 2005, 2013; V. Iršič et al. 2017; B. Villanor et al. 2023), or FDM mass up to  $\sim 10^{-21} - 10^{-23} \text{ eV}$  (H. Lazare et al. 2024; J. Sipple et al. 2025). But the power spectrum at  $k \gtrsim 10 \text{ Mpc}^{-1}$  is still not known. In the future, with the Square Kilometre Array (SKA) telescope, the 21 cm forest could be a powerful probe for either the damping (H. Shimabukuro et al. 2020a; Y. Shao et al. 2023) or the enhancement (H. Shimabukuro et al. 2020b) of the small structures before the end of reionization.

Reionization is the last global phase transition in the history of the Universe, during which the intergalactic medium (IGM) evolves from a predominantly neutral state to a fully ionized plasma, driven by ionizing photons from the first stars, galaxies and black holes (R. Barkana & A. Loeb 2001). In the standard  $\Lambda$ CDM scenario, ionizing photons are primarily provided by star-forming galaxies in dark matter halos with virial temperature  $T_{\text{vir}} \gtrsim 10^4 \text{ K}$ , corresponding to halo masses  $M_{\text{h}} \gtrsim 10^8 M_{\odot}$  in the epoch of reionization (EoR) (J. Witstok et al. 2025; Z. Wu & A. Kravtsov 2024; N. Choustikov et al. 2025). However, a population of lower-mass halos with  $T_{\text{vir}} \lesssim 10^4 \text{ K}$ , named minihalos, also plays a critical role in reionization process. While a fraction of minihalos with  $10^3 \text{ K} \lesssim T_{\text{vir}} \lesssim 10^4 \text{ K}$  may host Pop III stars (R. S. Klessen & S. C. O. Glover 2023), most of them have no chance to host any stars before virial temperature exceeding  $10^4 \text{ K}$  and Hydrogen atomic-cooling being efficient. Their primary impact on reionization is as potent sinks of ionizing photons, owing to recombinations in their dense, self-shielded gas (R. Barkana & A. Loeb 2002; P. R. Shapiro et al. 2004; I. T. Iliev et al. 2005; B. Ciardi et al. 2006; B. Yue et al. 2009; Y. Mao et al. 2020). This sink behavior arises

from two key mechanisms: self-shielding and enhanced recombination. Self-shielding occurs due to high gas densities that shield interiors from ionizing radiation, trapping ionization fronts (P. R. Shapiro et al. 2004; I. T. Iliev et al. 2005); while enhanced recombination results from elevated densities that increase recombination rates, leading to a large amount of ionizing photons consumption (T. K. Chan et al. 2024). If the power spectrum at small scales is enhanced compared to the regular  $\Lambda$ CDM model, then either the production of ionizing photons by faint galaxies, or the consumption of ionizing photons by minihalos, or both of them, would be boosted. The net impact on reionization depends on the competition between the two effects, and the large-scale morphology of the ionization field would change. Observing the large-scale morphology of the ionization field provides potential possibility to detect power spectrum at small scales.

In the Dark Ages, the 21 cm emission line from neutral Hydrogen traces the density field very well, it can directly detect small-scale structures provide that the telescope has high angular resolution (A. Loeb & M. Zaldarriaga 2004; P. S. Cole & J. Silk 2021). More promisingly, even without directly resolving structures at these scales, the large-scale power spectrum of the 21 cm signal also tells us the information of them in the Dark Ages and the Cosmic Dawn (Y. Ali-Haïmoud et al. 2014; J. B. Muñoz et al. 2020; X. Zhang et al. 2023; S. Sikder et al. 2025). This is also the case for the EoR, where the 21 cm signal measures the large-scale morphology of the ionization field (e.g. S. R. Furlanetto et al. 2006; J. R. Pritchard & A. Loeb 2012) and provide us with information of faint galaxies and minihalos at small scales.

In this paper, we investigate the galaxy UV LFs at the EoR, the CMB scattering optical depth, the reionization history, the 21 cm power spectrum and bubble size distribution (BSD) in a small-scale enhanced power spectrum model proposed by M. Cielo et al. (2025) (C25 hereafter). We compare these results with the regular  $\Lambda$ CDM model and estimate the detectability of their differences for the upcoming SKA-low AA\* and an assumed further telescope that is able to do tomographic imaging observations. This paper is organized as follows: in Section 2, we introduce our methods for constructing the UV LFs of galaxies during the EoR from the power spectrum model, and for building ionization and 21 cm fields using the semi-numerical algorithm. We take into account the boost in both ionizing photons production by faint galaxies, and consumption by minihalos. In Section 3, we present our results on the reionization history, the 21 cm power spectrum, and the

BSD. We also analyze the detectability of the small-scale power spectrum effects through these quantities. We give the summary and discussion in Section 4. Throughout this paper, we adopt cosmological parameters from Planck18 release, say  $(\Omega_m, \Omega_b, \Omega_\Lambda, h, \sigma_8, n_s) = (0.315, 0.0493, 0.685, 0.674, 0.811, 0.965)$  (Planck Collaboration et al. 2020).

## 2. METHODS

In this section, we introduce the model proposed in M. Cielo et al. (2025), for which the small-scale density fluctuations are enhanced compared to the regular  $\Lambda$ CDM model. We then calculate the UV LFs and ionization fields in such a model, and the corresponding 21 cm signal fields.

### 2.1. The C25 model and halo mass function

M. Cielo et al. (2025) proposed a model for which the primordial scalar power spectrum is enhanced on small scales by sudden phase transitions during inflation. Considering de Sitter-invariant initial state for the inflaton field in  $\alpha$  vacua (B. Allen 1985) - which can be excited by preceding transitions - M. Cielo et al. (2025) find a  $\sim k^6$  growth in a large volume of parameter space.

For de Sitter-invariant initial state in  $\alpha$  vacua, the normalization and phase difference of Bogoliubov coefficients are parameterized by two real parameters  $\alpha$  and  $\beta$ , respectively. In the simplified case where the phase difference vanishes ( $\beta = 0$ ), and when the phase transition is modeled as a sudden change in the slope of the inflaton potential, the primordial scalar power per e-fold is given by

$$\Delta_{\text{C25}}^2(k) = \frac{9H^6}{4\pi^2 A_1^2 A_2^2} \left\{ e^{-2\alpha} \left[ A_1 + 3(A_1 - A_2) \frac{(\kappa^2 - 1) \sin(2\kappa) + 2\kappa \cos(2\kappa)}{2\kappa^3} \right]^2 + e^{2\alpha} [3(A_1 - A_2)\kappa j_1^2(\kappa)]^2 \right\}, \quad (1)$$

where  $A_1$  and  $A_2$  are respectively the pre- and post-transition potential slopes, and  $j_1$  is the spherical Bessel function of order 1. The dimensionless wavenumber  $\kappa$  is defined as  $k/k_{\text{trans}}$ , where  $k_{\text{trans}}$  is the comoving horizon scale at the phase transition. The term  $9H^6/(4\pi^2 A_1^2 A_2^2)$  in the right-hand side of Eq. (1) is a normalization factor in perfect de Sitter background. In more realistic slow-roll scenarios, this normalization factor slowly varies and can be approximated as a power-law function with spectral index  $n_s - 1$ , whose amplitude is much smaller than 1.

For large excitation ( $\alpha \gg 0$ ) and a strong transition ( $A_1 \gg A_2$ ), the spectrum can grow as  $\Delta_{\text{C25}}^2(k) \propto k^6$  before reaching a peak, significantly exceeding the  $k^4$  scaling in the case of no excitation ( $\alpha = 0$ , Bunch-Davies vacuum). In the absence of phase transition ( $A_1 = A_2$ ) and with the incoming state being Bunch-Davies vacuum, the power spectrum reduces into the regular nearly scale-invariant model. To conduct a concrete study of this model, throughout this paper we take representative parameter values  $A_2/A_1 = 0.1$  and  $\alpha = 2$  which give rise to the  $k^6$  growth, and only vary  $k_{\text{trans}}$ .

The linear matter power spectrum in this C25 model can be obtained by rescaling the primordial scalar power spectrum,

$$P_{\text{C25}}(k, z) = P(k, z) \times \frac{\Delta_{\text{C25}}^2(k)}{\Delta^2(k)}, \quad (2)$$

where  $P(k, z)$  and  $\Delta^2(k)$  are matter power spectrum and dimensionless primordial power spectrum in the regular  $\Lambda$ CDM model respectively. We calculate  $P(k, z)$  and  $\Delta^2(k)$  from CAMB (A. Lewis et al. 2000) for  $k < 100 \text{ Mpc}^{-1}$ , and extrapolate to higher  $k$  using the fitting formula BBKS (J. M. Bardeen et al. 1986). In Figure 1 we plot the matter power spectrum at  $z = 6$  for the regular  $\Lambda$ CDM model, used as the fiducial model in this paper, and for the C25 models with different  $k_{\text{trans}}$  values. In the C25 model, the matter power spectrum is significantly enhanced at small scales. Toward small scales, it starts to obviously deviate from the fiducial model at  $k_{\text{start}} \sim 0.15k_{\text{trans}}$ ; reaches a peak and forms a ‘‘bump’’ at  $k_{\text{bump}} \sim 1.9k_{\text{trans}}$ ; and then extends to much smaller scales.

With the matter power spectrum, we then calculate the halo mass function from the Sheth & Tormen formalism (R. K. Sheth & G. Tormen 1999),

$$\frac{dn}{dM_h}(M_h, z) = \rho_m \frac{1}{M_h} \frac{1}{\sigma(M_h)} \left| \frac{d\sigma(M_h)}{dM_h} \right| f_{\text{ST}}(\sigma, z) \quad (3)$$

for which

$$f_{\text{ST}}(\sigma, z) = A \sqrt{\frac{2a}{\pi}} \left[ 1 + \left( \frac{\sigma^2}{a\delta_c^2} \right)^p \right] \frac{\delta_c}{\sigma} \exp\left(-\frac{a\delta_c^2}{2\sigma^2}\right), \quad (4)$$

and

$$\sigma^2(M_h, z) = \frac{1}{2\pi^2} \int_0^\infty k^2 P(k) W^2(k, M_h) dk. \quad (5)$$

In above equations,  $\delta_c = 1.686/D(z)$  is the halo collapse threshold linearly extrapolated to  $z = 0$ . Parameters  $A = 0.353$ ,  $a = 0.73$ , and  $p = 0.175$  are fitted from the  $N$ -body simulations (A. Jenkins et al. 2001).

In Figure 2 we show the halo mass functions in the fiducial model and the C25 models with different  $k_{\text{trans}}$  values.

Compared with the fiducial model, in the C25 model the number of halos is significantly boosted in a certain mass range, but heavily depressed at the mass scale much smaller than this range. From higher mass to lower mass, the mass function starts to be obviously boosted at the mass scale corresponding to  $k_{\text{start}}$ ,

$$\begin{aligned} M_{\text{h}}^{\text{start}} &\sim \rho_{\text{m}} \frac{4\pi}{3} \left( \frac{2\pi}{k_{\text{start}}} \right)^3 \\ &\approx \rho_{\text{m}} \frac{4\pi}{3} \left( \frac{2\pi}{0.15k_{\text{trans}}} \right)^3 \\ &\approx 300\rho_{\text{m}} \frac{4\pi}{3} \left( \frac{2\pi}{k_{\text{trans}}} \right)^3. \end{aligned} \quad (6)$$

The boost keeps increasing until a mass point  $M_{\text{h}}^{\text{bend}}$ , then the halo mass function in the C25 model starts bend to the fiducial model. Below  $\sim M_{\text{h}}^{\text{bend}}$ , in the C25 model the halo number density grows more slowly than in the fiducial model, and finally becomes lower than the fiducial model.

From a mathematical perspective, according to Eqs. (3 & 4), the halo number density is primarily governed by the term  $|\text{d}\sigma/\text{d}M_{\text{h}}|/\sigma^{2(1-p)}$ . In the fiducial model, this term gradually grows with decreasing  $M_{\text{h}}$ . In the C25 model, when  $M_{\text{h}}$  is approaching  $M_{\text{h}}^{\text{bend}}$  from the higher mass side, both  $|\text{d}\sigma/\text{d}M_{\text{h}}|$  and  $\sigma^{2(1-p)}$  rise to higher than the fiducial model. At the beginning,  $|\text{d}\sigma/\text{d}M_{\text{h}}|$  increases faster than  $\sigma^{2(1-p)}$ , so the halo number density grows more rapidly than the fiducial model. However, when  $M_{\text{h}}$  drops to  $\lesssim M_{\text{h}}^{\text{bend}}$ ,  $\sigma^{2(1-p)}$  exhibits a steep rise. So the growth rate of the ratio  $|\text{d}\sigma/\text{d}M_{\text{h}}|/\sigma^{2(1-p)}$  slows down to below the fiducial model.

To derive the  $M_{\text{h}}^{\text{bend}}$ , we note that the behavior of  $\sigma^{2(1-p)}$  is similar to  $\sigma^2$ . From the Eq. (5), the contribution of the power spectrum to the  $\sigma^2$  is controlled by the window function  $W^2(k, M_{\text{h}})$ . Only when  $k \lesssim 0.5 \times 2\pi/R_{M_{\text{h}}}$ , where  $R_{M_{\text{h}}}$  is the radius scale of the mass  $M_{\text{h}}$ , the modes have sufficient contribution in the  $\sigma^2$ . Therefore the  $\sigma^2$  starts to increase suddenly only when the modes with enhanced power spectrum ( $k \gtrsim k_{\text{start}}$ ) is covered by the window function. So the bend point must satisfy

$$k_{\text{start}} \sim 0.15k_{\text{trans}} \lesssim 0.5 \frac{2\pi}{R_{M_{\text{h}}^{\text{bend}}}}. \quad (7)$$

Therefore

$$\begin{aligned} M_{\text{h}}^{\text{bend}} &= \rho_{\text{m}} \frac{4\pi}{3} R_{M_{\text{h}}^{\text{bend}}}^3 \\ &\sim \rho_{\text{m}} \frac{4\pi}{3} \left( \frac{2\pi}{0.3k_{\text{trans}}} \right)^3 \\ &\approx 40\rho_{\text{m}} \frac{4\pi}{3} \left( \frac{2\pi}{k_{\text{trans}}} \right)^3. \end{aligned} \quad (8)$$

Physically speaking, in the C25 model, although the matter power spectrum enhancement boosts the collapse probability at all mass scales, it also accelerates the hierarchical merger process. Smaller halos merge into larger ones more frequently and even induces a deficit of smaller halos in the C25 model compared with the fiducial model. Actually, similar phenomenon is also observed in the fiducial model itself. Although the matter power spectrum increases monotonously with decreasing redshift, at  $z \sim 0$ , the number density of halos below  $\sim 10^7 M_{\odot}$  is even smaller than higher redshifts, because of the hierarchical merger.

Explicitly, for  $k_{\text{trans}} = 100 \text{ Mpc}^{-1}$ , in the EoR halos with mass  $10^6 M_{\odot} \lesssim M_{\text{h}} \lesssim 10^{10} M_{\odot}$  are enhanced, while halos with mass  $M_{\text{h}} \lesssim 10^6 M_{\odot}$  are depressed. In this case the faint-end of the UV LFs will be enhanced, and quite likely that reionization will be promoted. For  $k_{\text{trans}} = 200 \text{ Mpc}^{-1}$ , in the mass range  $10^5 M_{\odot} \lesssim M_{\text{h}} \lesssim 10^9 M_{\odot}$  halos are enhanced and, below  $10^5 M_{\odot}$  halos are depressed. The UV LFs at the faint-end will be enhanced but the reionization is more complicated. We will see later on that in this case, reionization is promoted at the beginning, however be delayed at the late stage of the EoR. For  $k_{\text{trans}} = 400 \text{ Mpc}^{-1}$ , halos in  $10^5 M_{\odot} \lesssim M_{\text{h}} \lesssim 10^8 M_{\odot}$  are enhanced. This mass range is below the minimum halo mass for galaxy formation and entirely confined to minihalo mass. Then the UV LFs are not influenced but the reionization process will be delayed, as the minihalos would consume ionizing photons.

## 2.2. The UV LFs

Similar to M. Zhang et al. (2025), we derive the UV LFs from halo mass functions, based on SFR- $M_{\text{h}}$  and  $L_{\text{UV}}$ -SFR relations, where  $L_{\text{UV}}$  is the UV luminosity defined at  $1600 \text{ \AA}$ , and SFR is the star formation rate. The SFR- $M_{\text{h}}$  relation is expressed as:

$$\text{SFR}(M_{\text{h}}, z) = f_*(M_{\text{h}}, z) \frac{\Omega_b}{\Omega_m} \dot{M}_{\text{h}}, \quad (9)$$

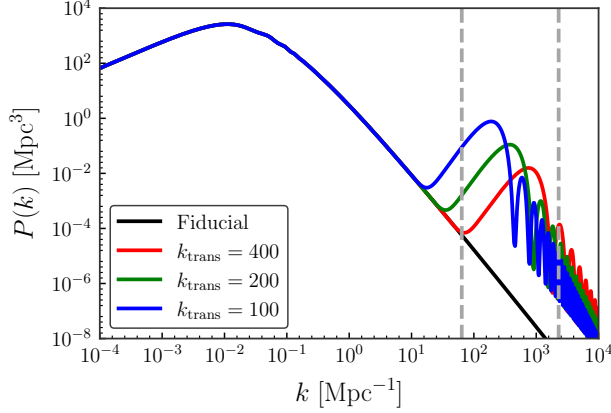


**Figure 1.** The power spectrum at  $z = 6$  for the fiducial model (regular  $\Lambda$ CDM model) and the C25 model with different  $k_{\text{trans}}$  values. The vertical dashed lines refer to scales of different typical masses: the left line corresponds to the virial mass at virial temperature  $T_{\text{vir}} = 10^4$  K, set as the lower mass limit for reionization sources and upper limit of minihalos; the right line corresponds to the Jeans mass, representing the minimal mass of minihalos hosting gas.

where the dark matter halo accretion rate (J. McBride et al. 2009)

$$\dot{M}_h(M_h, z) = 24.1 \left( \frac{M_h}{10^{12} M_\odot} \right)^{1.094} \times (1 + 1.75z) \sqrt{\Omega_m (1+z)^3 + \Omega_\Lambda} [M_\odot \text{ yr}^{-1}] \quad (10)$$

is fitted from N-body simulations, and the star formation efficiency,  $f_*$ , follows the double power law formalism (e.g. S. Tacchella et al. 2018):

$$f_*(M_h) = 2f_0 \left[ \left( \frac{M_h}{M_c} \right)^{-\gamma_{\text{lo}}} + \left( \frac{M_h}{M_c} \right)^{\gamma_{\text{hi}}} \right]^{-1}. \quad (11)$$

Here  $f_0 = 0.12$  is the star formation efficiency at the characteristic mass  $M_c = 10^{11.7} M_\odot$ ,  $\gamma_{\text{lo}} = 0.66$  and  $\gamma_{\text{hi}} = 0.65$  are low-mass and high-mass slopes respectively.

For a halo with mass  $M_h$  at redshift  $z$ , we assume that the log of UV luminosity has a Gaussian distribution around a central value,

$$P_{\log L_{\text{UV}}} = \frac{1}{\sqrt{2\pi}\sigma_{\text{UV}}} \exp\left(-\frac{(\log L_{\text{UV}} - \log \hat{L}_{\text{UV}})^2}{2\sigma_{\text{UV}}^2}\right), \quad (12)$$

where we set the scatter  $\sigma_{\text{UV}} = 0.30$  and  $\hat{L}_{\text{UV}}$  is given by

$$\hat{L}_{\text{UV}} = \text{SFR}/\mathcal{K}_{\text{UV}}, \quad (13)$$

and  $\mathcal{K}_{\text{UV}} = 1.17 \times 10^{-28} M_\odot \text{ yr}^{-1}/(\text{erg s}^{-1} \text{ Hz}^{-1})$  (M. Zhang et al. 2025).

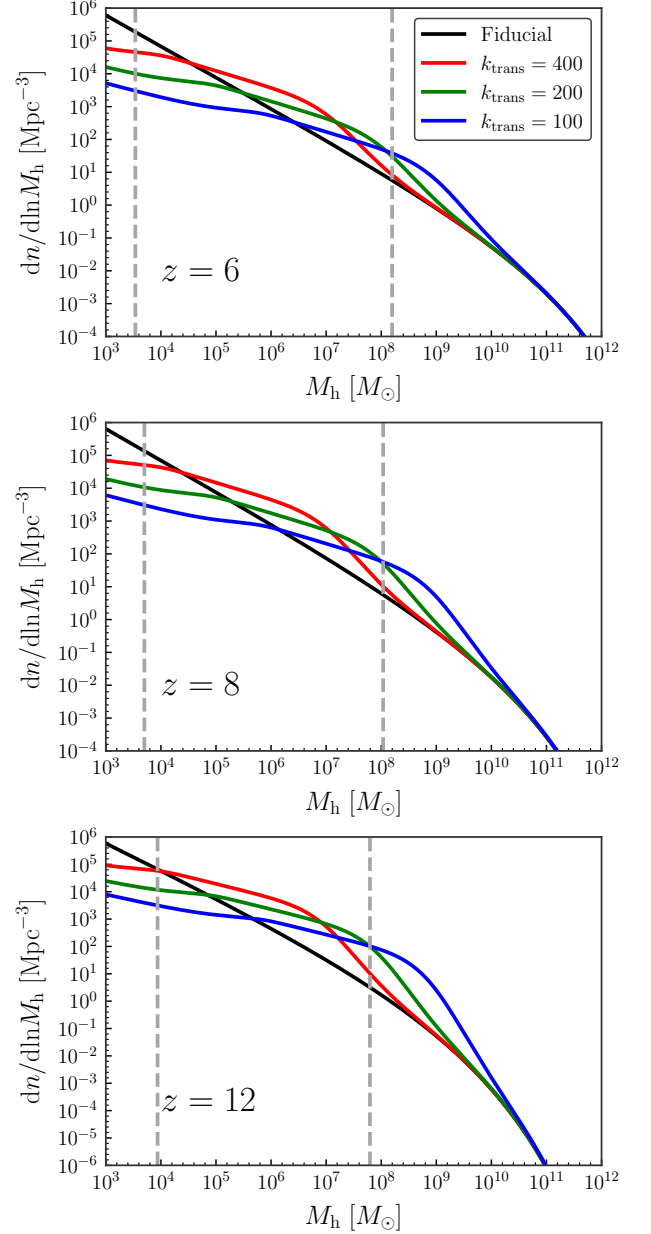


**Figure 2.** Halo mass functions for fiducial model and C25 model with different  $k_{\text{trans}}$  values at the EoR. In each panel, the left vertical line refers to the Jeans mass, which is the minimal mass of minihalos able to retain gas; the right vertical line corresponds to virial mass of  $T_{\text{vir}} = 10^4$  K, set as the lower mass limit for reionization sources and upper limit of minihalos.

The UV LF is obtained by integrating over halo mass:

$$\frac{dn}{d \log L_{\text{UV}}} = \int_{M_{\text{min}}}^{\infty} dM_h f_{\text{duty}}(M_h, z) \frac{dn}{dM_h} P_{\log L_{\text{UV}}} \quad (14)$$

where  $M_{\text{min}}$  is the minimum mass of halos allowing galaxy formation, and we adopt the virial mass corresponding to virial temperature  $10^4$  K (R. Barkana & A.

Loeb 2001).

$$f_{\text{duty}}(M_{\text{h}}, z) = \exp\left(-\frac{M_{\text{turn}}(z)}{M_{\text{h}}}\right), \quad (15)$$

is the duty cycle (J. Park et al. 2019), i.e., only a fraction  $f_{\text{duty}}$  of halos host active star formation. The turnover threshold mass (H. A. G. Cruz et al. 2025)

$$M_{\text{turn}}(z) = 3.3 \times 10^7 \left[\frac{(1+z)}{21}\right]^{-3/2} M_{\odot}. \quad (16)$$

We further add the dust effects via

$$M_{\text{UV}} = M_{\text{UV}}^{\text{obs}} - A_{\text{UV}}, \quad (17)$$

where the dust attenuation

$$A_{\text{UV}} = C_1 + C_0\beta, \quad (A_{\text{UV}} \geq 0). \quad (18)$$

We adopt the coefficients  $C_0 = 2.10$  and  $C_1 = 4.85$  (M. P. Koprowski et al. 2018), and the UV spectral slope  $\beta$  is taken from M. Vogelsberger et al. (2019).

In Figure 3 we show the predicted UV LFs for the fiducial model and the C25 models with different  $k_{\text{trans}}$  values, compared with the observations of HST and JWST (R. J. McLure et al. 2013; S. L. Finkelstein et al. 2015; R. A. A. Bowler et al. 2020; R. J. Bouwens et al. 2021; Y. Harikane et al. 2023; R. J. Bouwens et al. 2023; C. T. Donnan et al. 2023, 2024). The  $L_{\text{UV}}$  is converted to absolute UV magnitude.

In the fiducial model, the predicted UV LFs agree with the observations very well, and as long as  $k_{\text{trans}} \gtrsim 100$  Mpc $^{-1}$ , UV LFs in C25 models are also consistent with observations. Interestingly, at the redshifts  $\gtrsim 12$ , the UV LFs in C25 models agree with observations better than the fiducial model, providing a potential solution for the excess of high redshift galaxy population in JWST observations (e.g. A. Adamo et al. 2025; Y. Harikane et al. 2023).

In our model, the typical absolute UV magnitude of the minimum halo mass allowing star formation,  $\hat{M}_{\text{UV}}$ , is  $\sim -7$ , where  $\hat{M}_{\text{UV}}$  is the absolute magnitude of the central UV luminosity  $\hat{L}_{\text{UV}}$  in Eq. (12), and this value just changes slightly in the redshift range considered in this paper. However, because we assume real magnitudes  $M_{\text{UV}}$  follow Gaussian distribution around this central value, the faintest magnitude can extend to far below this central value, just the probability is very small. At the faint-end, the UV LFs in Figure 3 start to deviate from the power-law faint-end in the popular Schechter formula (e.g. R. J. Bouwens et al. 2015; S. L. Finkelstein et al. 2015) at  $M_{\text{UV}}$  from  $\sim -13$  to  $-8$ . This is broadly consistent with predictions in semi-analytical models (e.g. L. Y. A. Yung et al. 2019) and

simulations (e.g. P. Ocvirk et al. 2020). We note that in many simulations the UV LFs drop dramatically below  $M_{\text{UV}} \sim -10$  (e.g. N. Y. Gnedin 2016), however our UV LFs still gradually grow or at least keeps flat until  $M_{\text{UV}} \sim -7$ , probably because we do not model the complicated feedback mechanisms. Currently, the deep observations with strong gravitational lensing probe the UV LFs down to magnitudes as faint as  $M_{\text{UV}} \sim -13$  (e.g., H. Atek et al. 2018; M. Ishigaki et al. 2018; R. J. Bouwens et al. 2022). Other works aiming to reconstruct the EoR UV LFs from the observations of local dwarf galaxies extend the faintest magnitudes down to  $\sim -5$  (e.g. D. R. Weisz et al. 2014). But none of those works have yet confirmed the deviation from the power-law, as the uncertainties are still large (R. C. Livermore et al. 2017; R. J. Bouwens et al. 2017; B. Yue et al. 2018). The shape of the UV LFs faint-end reflects the feedback mechanisms that are more efficient in smaller halos (B. Yue et al. 2016). It can be described by involving more sophisticated models of the duty-cycle, star formation mode and efficiency in our model.

### 2.3. The reionization process and the 21 cm signal

To compute the 21 cm brightness temperature field in the EoR, we first generate the ionization field using a semi-numerical excursion-set approach (S. R. Furlanetto et al. 2004; A. Mesinger et al. 2011). In the excursion-set framework, a spherical region with radius  $R$  is ionized as long as the cumulative number of ionizing photons escaped into the IGM is larger than the consumptions by both the IGM and minihalos,

$$N_{\text{ion}}(z|R, \delta_R) \geq (1 + \bar{n}_{\text{rec}}) N_{\text{H}}(\delta_R)(1 - f_{\text{coll}}(z > M_{\text{J}})) + N_{\xi}(z|R, \delta_R), \quad (19)$$

where  $N_{\text{ion}}(z|R, \delta_R)$  denotes the cumulative number of ionizing photons that have escaped into the IGM for a spherical region with smoothed overdensity  $\delta_R$  and radius  $R$ ,  $\bar{n}_{\text{rec}}$  is the mean cumulative number of recombinations per Hydrogen atom in the IGM,  $N_{\text{H}}(\delta_R)$  is the number of neutral atoms in the region, and  $f_{\text{coll}}(> M_{\text{J}})$  is the collapse fraction of halos above Jeans mass (R. Barkana & A. Loeb 2001). Compared with the standard excursion-set model, here we add the ionizing photons consumed by minihalos inside the spherical region,  $N_{\xi}$ .

The cumulative number of ionizing photons

$$N_{\text{ion}} = V \int_{M_{\text{min}}}^{M_{\text{max}}} \left[ f_{\text{esc}} N_{\gamma/\text{b}} f_*(M_{\text{h}}, z) \frac{\Omega_{\text{b}}}{\Omega_{\text{m}}} M_{\text{h}} \times f_{\text{duty}}(M_{\text{h}}, z) \frac{dn}{dM_{\text{h}}}(M_{\text{h}}, z|\delta_R, M_{\text{R}}) \right] dM_{\text{h}} \quad (20)$$

where  $V$  is the region volume,  $M_{\text{max}}$  is the maximum mass of halos in the spherical region,  $f_{\text{esc}}$  is the es-

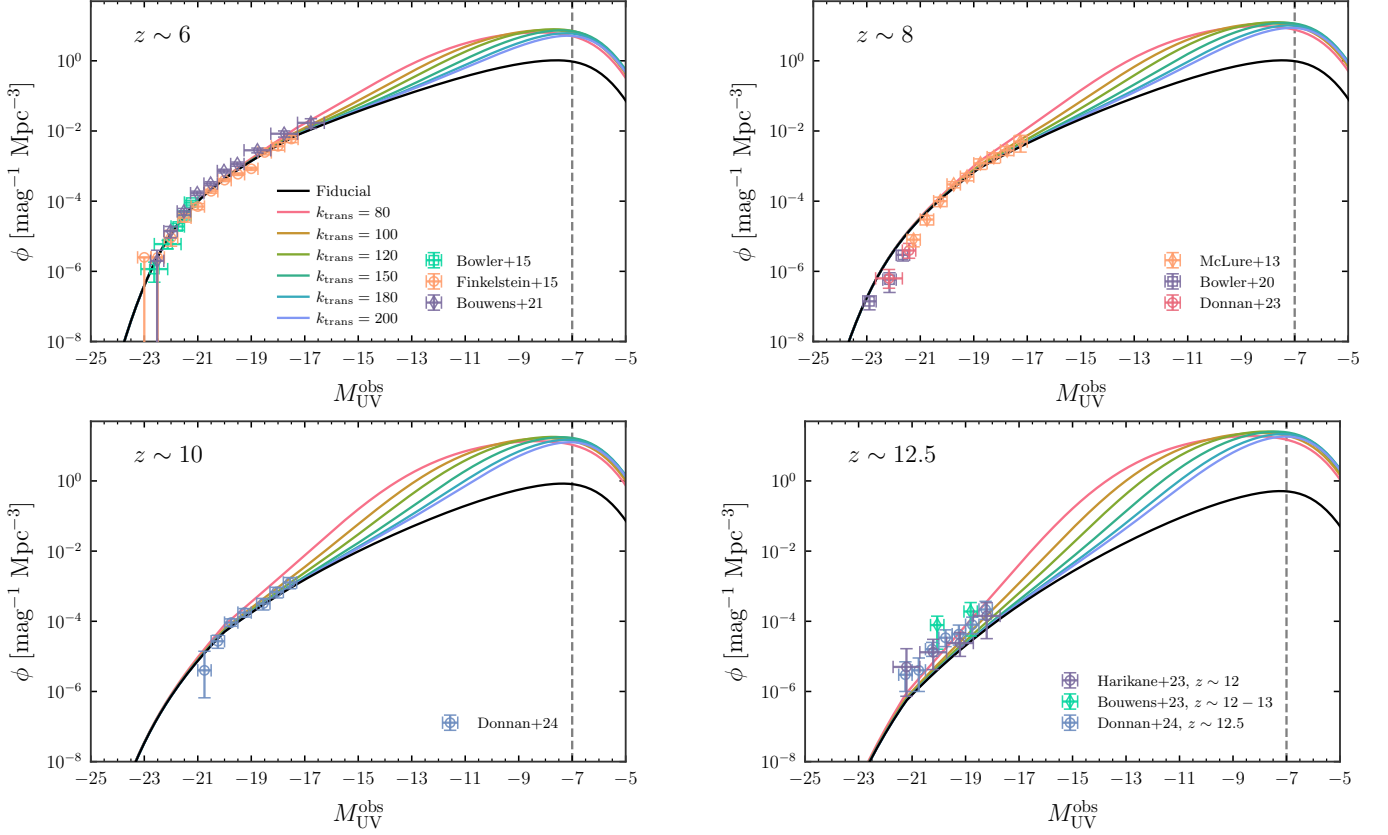


**Figure 3.** The predicted UV LFs in fiducial model and in C25 models with different values of  $k_{\text{trans}}$ , compared with observations (R. J. McLure et al. 2013; S. L. Finkelstein et al. 2015; R. A. A. Bowler et al. 2020; R. J. Bouwens et al. 2021; Y. Harikane et al. 2023; R. J. Bouwens et al. 2023; C. T. Donnan et al. 2023, 2024). The vertical dashed line in each panel indicates the central absolute UV magnitude corresponding to the minimum halo mass required for star formation,  $\hat{M}_{\text{UV}} \sim -7$ .

cape fraction, and  $N_{\gamma/b}$  is the number of ionizing photons per stellar baryon produced in their lifetime, for which we adopt 9,500, provided by Starburst99 (C. Leitherer et al. 1999; G. A. Vázquez & C. Leitherer 2005; C. Leitherer & J. Chen 2009; C. Leitherer et al. 2014) for a Kroupa IMF (P. Kroupa 2001) and metallicity  $Z = 0.05Z_{\odot}$ . The conditional mass function  $\frac{dn}{dM_h}(M_h, z|\delta_R, M_R)$  is provided by the Extended Press-Schechter (EPS) formalism (H. J. Mo & S. D. M. White 1996). Similar to 21cmFAST (A. Mesinger et al. 2011), we normalize the mean number density of ionizing photons in the Universe to the values given by Sheth & Tormen halo mass function. Throughout this paper, we set  $M_{\text{max}} = \min(10^{15} M_{\odot}, 0.9M_R)$ , where  $M_R$  is the mass of the spherical region.

The gas numbers in the spherical region with volume  $V$  simply

$$N_{\text{H}} = \frac{V}{\mu_{\text{b}} m_{\text{H}}} \bar{\rho}_{\text{b}} (1 + \delta_R), \quad (21)$$

where  $\bar{\rho}_{\text{b}}$  is the mean comoving baryon density of the Universe,  $\mu_{\text{b}}$  is the mean molecular weight and  $m_{\text{H}}$  is the mass of Hydrogen atom.

The recombination numbers  $\bar{n}_{\text{rec}}$  is solved from the following differential equation (T. R. Choudhury & A. Chakraborty 2025),

$$\frac{dn_{\text{rec}}}{dt} = \chi_{\text{He}} C_{\text{HII}} n_{\text{H}} X_{\text{HII}} \alpha_{\text{A}} (T_{\text{HII}}) (1+z)^3, \quad (22)$$

where  $\chi_{\text{He}} \approx 1.08$  is the contribution of singly-ionized Helium to the free electron density,  $n_{\text{H}}$  is the comoving Hydrogen number density,  $C_{\text{HII}}$  is the IGM clumping factor (J. M. Shull et al. 2012),

$$C_{\text{HII}} = 2.9[(1+z)/6]^{-1.1}, \quad (23)$$

and  $\alpha_{\text{A}}$  is the Case A recombination coefficient. To simplify the calculation, we assume the IGM temperature  $T_{\text{HII}} = 10^4$  K that gives  $\alpha_{\text{A}} = 4.2 \times 10^{-13}$ . The quantity of the  $n_{\text{rec}}$  at redshift  $z$  is obtained simply by integrating Eq. (22) from  $\infty$  to  $z$ :

$$n_{\text{rec}} = \int_{\infty}^z dz \frac{dt}{dz} \frac{dn_{\text{rec}}}{dt}. \quad (24)$$

The number of photons consumed by minihalos

$$N_{\xi}(z|R, \delta_R) = V \int_{M_J}^{M_{\min}} \left[ \xi(M_h, z) \frac{1}{\mu_b m_H} \frac{\Omega_b}{\Omega_m} M_h \right. \\ \left. \times \frac{dn}{dM_h}(M_h, z|\delta_R, M_R) \right] dM_h, \quad (25)$$

where  $\xi(M_h, z)$  is the mean number of ionizing photons consumed per Hydrogen atom until a minihalo is completely photo-evaporated by the ionization front (I. T. Iliev et al. 2005).

We use the 21cmFAST (A. Mesinger & S. Furlanetto 2007; A. Mesinger et al. 2011; J. Park et al. 2019; S. Murray et al. 2020) to generate density fields for both fiducial model and the C25 models, following the Zel’dovich approximation algorithm (Y. B. Zel’dovich 1970). The density fields have box size 300 Mpc and  $300^3$  cells. We then apply the above excursion-set algorithm to the density fields, to generate the ionizing fields. This is also analogous to 21cmFAST. Explicitly, We adopt a series of smoothing radii  $R$  ranging from 50 Mpc down to 1 Mpc. For each cell, starting from the largest smoothing radius, we check if the ionization condition Eq. (19) is satisfied. If it is satisfied, then the cell is marked as “ionized”, otherwise we move to smaller smoothing radius. If the cell remains neutral at the smallest radius, it is assigned a partial ionization fraction defined by the ratio of the LHS to the RHS of Eq. (19). This accounts for contributions of ionized bubbles smaller than the minimum smoothing radius. Such a treatment is not crucial for the fiducial model, as the contribution of partially ionized cells to the total ionization fraction is  $\sim 0.15$ . However, in the C25 model it is important, because the matter power spectrum enhancement at small scales largely boosts the number of minihalos and the ionization barrier. It trends to form more smaller ionized bubbles rather than fewer larger bubbles. For example, when  $k_{\text{trans}} = 150 \text{ Mpc}^{-1}$ , the contribution to the total ionization fraction from partially ionized cells is  $\sim 0.32$ . We remind, however, that the distinction between partial ionization and full ionization depends on resolution. A partially ionized cell in a lower resolution box will be split into some fully ionized cells and some neutral cells if increasing the resolution. Nevertheless, the power spectrum and the BSD at scales much larger than resolution will be less sensitive to this, but the integrated CMB scattering optical depth may be influenced.

We then calculate the 21 cm signal field from the ionization field. The 21 cm brightness temperature (S. R.

Furlanetto et al. 2004)

$$\delta T_b(\delta_b, z) \approx 27 X_{\text{HI}}(1 + \delta_b) \left( \frac{\Omega_b h^2}{0.023} \right) \left( \frac{0.15}{\Omega_m h^2} \frac{1+z}{10} \right)^{1/2} \\ \times \left( \frac{T_S - T_{\text{CMB}}}{T_S} \right) \text{ mK}, \quad (26)$$

where  $X_{\text{HI}}$  is the neutral Hydrogen fraction,  $T_S$  is the Hydrogen spin temperature,  $T_{\text{CMB}}$  is the CMB temperature. Throughout this paper, we limit our investigation in the EoR when the IGM has been heavily heated and Ly $\alpha$  scattering has been saturated, it is reasonable to assume that  $T_S \gg T_{\text{CMB}}$  (HERA Collaboration et al. 2023).

In Figure 4 we show the 21 cm signal fields at  $\langle X_{\text{HII}} \rangle = (0.25, 0.50, 0.75)$  for the fiducial model and the C25 models with  $k_{\text{trans}} = 400 \text{ Mpc}^{-1}$  and  $k_{\text{trans}} = 150 \text{ Mpc}^{-1}$  respectively, we set  $f_{\text{esc}} = 0.15$ . In the C25 model, these two  $k_{\text{trans}}$  values represent two different typical situations. For  $k_{\text{trans}} = 400 \text{ Mpc}^{-1}$ , only minihalos are boosted. So it purely enhances the consumption of ionizing photons, but the production of ionizing photons and the galaxy UV LFs are same to the fiducial model.

For  $k_{\text{trans}} = 150 \text{ Mpc}^{-1}$ , however, both minihalos and galaxies are boosted. This is a more complicated situation as the net effects depend on the competition between the enhancements on consumption and on production of ionizing photons. Moreover, according to Figure 3, although the observed UV LFs allow the  $k_{\text{trans}}$  be smaller than  $150 \text{ Mpc}^{-1}$ , we will see in the next section that, if  $k_{\text{trans}} \lesssim 150 \text{ Mpc}^{-1}$ , for  $f_{\text{esc}} = 0.15$  it may produce too many ionizing photons and break the constraints set by CMB scattering optical depth.

From Figure 4, we see that

for the C25 model with  $k_{\text{trans}} = 400 \text{ Mpc}^{-1}$  the 21 cm signal field is almost same to fiducial model as long as  $\langle X_{\text{HII}} \rangle$  is the same. However, for  $k_{\text{trans}} = 150 \text{ Mpc}^{-1}$ , the size of ionized regions are much smaller than the ‘fiducial model, even the mean ionization fraction  $\langle X_{\text{HII}} \rangle$  is the same.

Particularly, in this case when  $\langle x_{\text{HII}} \rangle = 0.25$  (see the top right panel of Figure 4), most of the contributions are from cells marked as “partially ionized”. However, we remind that partial ionization does not necessarily mean the mixed neutral and ionized atoms, instead, it actually refers to the volume fraction of fully ionized bubbles in that cell. The real partial ionization front of UV ionizing photons is quite thin and only occupies a small fraction in the volume. (e.g., I. T. Iliev et al. 2006b)

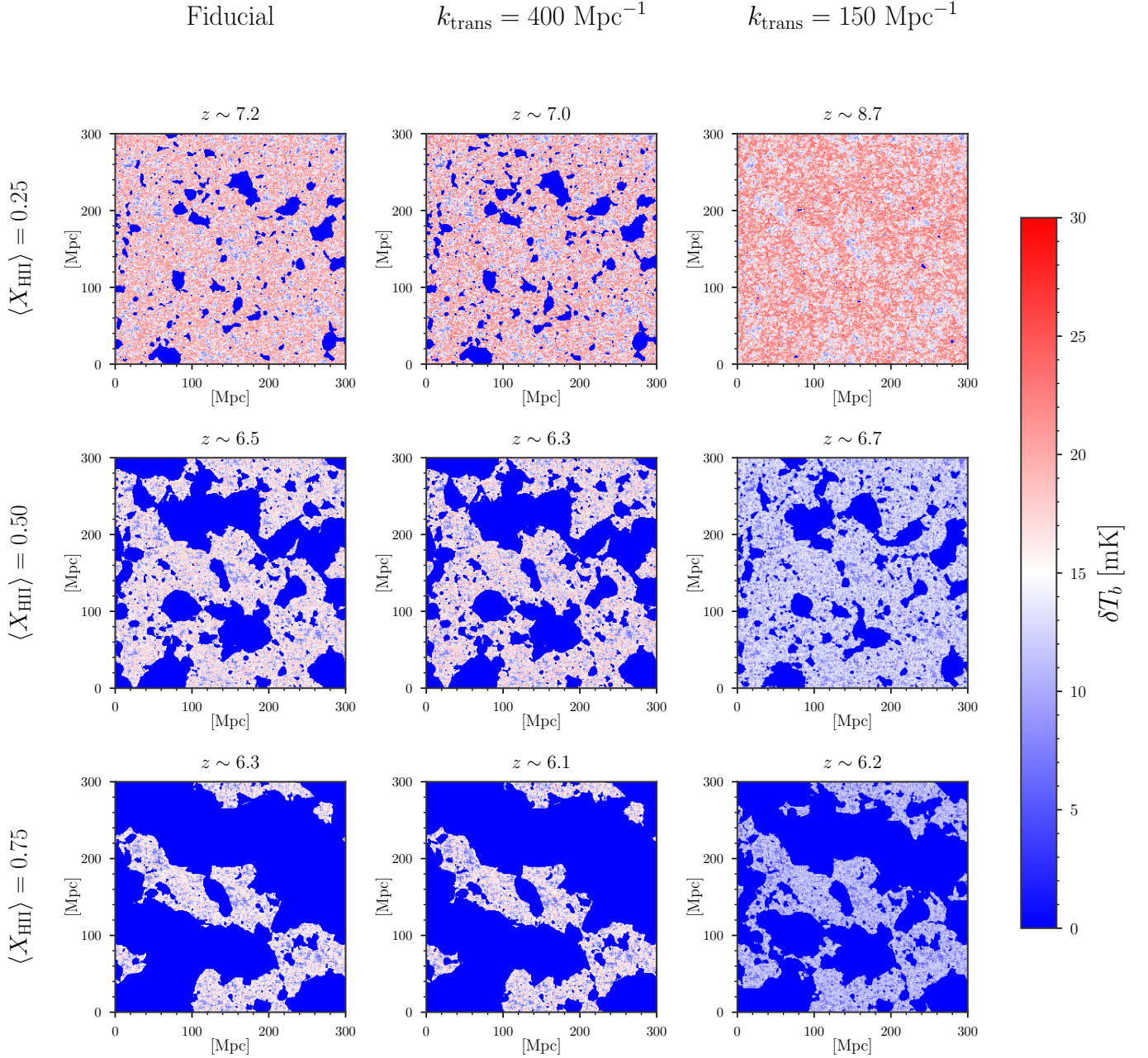


**Figure 4.** The 21 cm fields for fiducial model and C25 models with  $k_{\text{trans}} = 400 \text{ Mpc}^{-1}$  and  $k_{\text{trans}} = 150 \text{ Mpc}^{-1}$ . The first row displays the results for mean ionization fraction  $\langle X_{\text{HII}} \rangle = 0.25$ , the second row  $\langle X_{\text{HII}} \rangle = 0.50$  and the third row  $\langle X_{\text{HII}} \rangle = 0.75$ . The redshift of each panel is given above the top  $x$ -axis.

### 3. RESULTS

#### 3.1. The reionization history

The Thomson scattering optical depth to the CMB

$$\tau_e(z) = c\sigma_{\text{T}}\bar{n}_{\text{H}} \int_0^z \frac{(1+z')^2 dz'}{H(z')} \langle X_{\text{HII}} \rangle \left( 1 + \eta \frac{Y}{4X} \right), \quad (27)$$

where,  $c$  is the speed of light,  $\sigma_{\text{T}}$  is the Thomson cross-section,  $\bar{n}_{\text{H}}$  is the mean comoving number density of Hydrogen,  $H(z)$  is the Hubble parameter, and  $X$  and

$Y$  are the primordial mass fractions of Hydrogen and Helium, respectively. The  $\eta = 1$  ( $z > 3$ ) or  $\eta = 2$  ( $z < 3$ ) measures the degree of Helium ionization based on observations (J. M. Shull et al. 2010, 2012; P. R. Shapiro et al. 2004).

In Figure 5 we plot the  $\tau_e$  in fiducial model and the C25 models with different  $k_{\text{trans}}$  values, for different  $f_{\text{esc}}$ , compared with the observed  $\tau_e = 0.054 \pm 0.007$  (Planck Collaboration et al. 2020). In all cases the fiducial model always has optical depth consistent with observations.

Moreover, when  $f_{\text{esc}} = 0.10$ , models with  $k_{\text{trans}} \lesssim 130 \text{ Mpc}^{-1}$  are excluded by optical depth observations at  $2\sigma$  level. While when  $f_{\text{esc}} = 0.15$ , models with  $k_{\text{trans}} \lesssim 150 \text{ Mpc}^{-1}$ , and when  $f_{\text{esc}} = 0.25$ , models with  $k_{\text{trans}} \lesssim 180 \text{ Mpc}^{-1}$ , are excluded.

In Figure 6 we plot the reionization history in the fiducial model and the C25 models with different  $k_{\text{trans}}$  values, together with the neutral fractions in various observations (C. A. Mason et al. 2018, 2019; A. Hoag et al. 2019; S. Bruton et al. 2023; E. Curtis-Lake et al. 2023; B. Greig et al. 2022, 2024; H. Umeda et al. 2025; X. Jin et al. 2023). For  $f_{\text{esc}} = 0.10$  and 0.15, all models with  $k_{\text{trans}} \gtrsim 130 \text{ Mpc}^{-1}$  are consistent with observations. For  $f_{\text{esc}} = 0.25$ , it seems that reionization ended a bit earlier than, but still marginally consistent with, observations.

It is interesting to note that reionization history provides more information than the integrated variable  $\tau_e$ . For C25 models with  $130 \lesssim k_{\text{trans}} \lesssim 200 \text{ Mpc}^{-1}$ , the boost on ionizing photons production dominates over the boost on consumption, so the reionization is promoted at the early stage of the EoR ( $\langle X_{\text{HII}} \rangle \lesssim 0.3 - 0.6$ ), compared with the fiducial model. However, at the late stage of the EoR ( $\langle X_{\text{HII}} \rangle \gtrsim 0.3 - 0.7$ ), when most of regions have been ionized, boost on ionizing photons consumption in minihalos dominates over the production in halos  $> M_{\text{min}}$ , as a results the reionization is delayed.

In addition to the UV LFs, the CMB scattering optical depth and the reionization history put stricter constraints on the  $k_{\text{trans}}$  values in the C25 models. However, it is still infeasible to fully distinguish them, as the optical depth is an integration, while the observations of ionized fractions are still highly uncertain. We will investigate the possible constraints from 21 cm observations in following subsections.

### 3.2. The 21 cm power spectrum and detectability

Since in Figure 6, for  $f_{\text{esc}} = 0.25$  the reionization history is a bit earlier than observations, we adopt  $f_{\text{esc}} = 0.15$  in following calculations. We will no longer consider models with  $k_{\text{trans}} \lesssim 150 \text{ Mpc}^{-1}$ , as they are ruled out by the observed  $\tau_e$  when  $f_{\text{esc}} = 0.15$ . In Figure 7 we show the 21 cm power spectra in the fiducial model and the C25 models with different  $k_{\text{trans}}$  values, at redshifts  $z = 9.4, 7.6, 6.4$  and  $6.0$  respectively. We also plot the expected observational uncertainty levels for the SKA-low AA\*. The observational uncertainties are calculated by using the 21cmSense (J. C. Pober et al. 2013, 2014; S. G. Murray et al. 2024). We employ the SKA-low AA\* array within a 700 m radius, 8 MHz bandwidth and total 1080 hour integration. The 21cmSense provides three types of foreground removal modes: ‘‘Pessimistic’’,

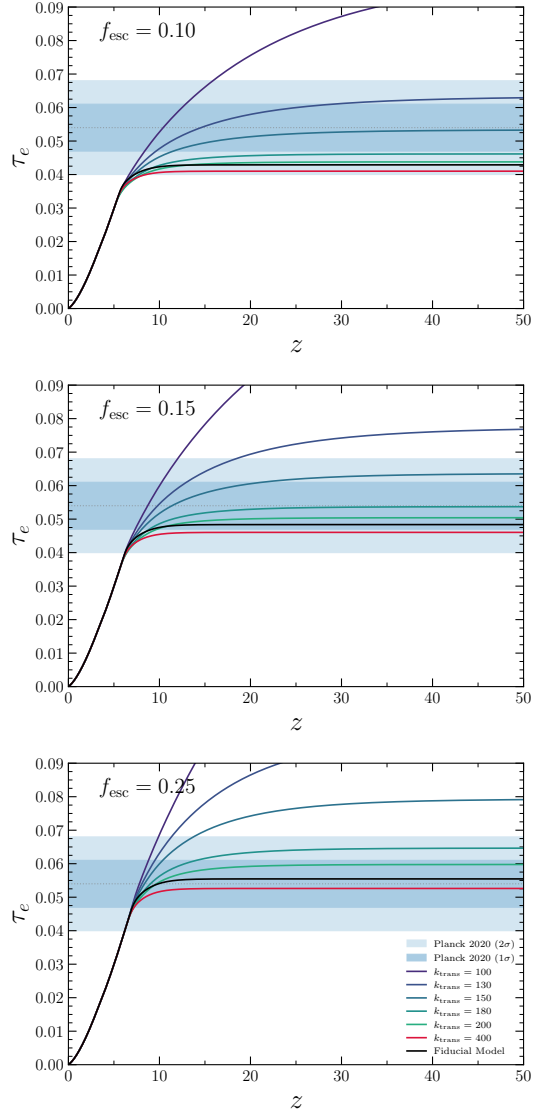


**Figure 5.** CMB scattering optical depth as a function of  $z$  for the fiducial model and C25 models with different  $k_{\text{trans}}$  values. The shaded filled regions are observational data and  $1\sigma$  and  $2\sigma$  uncertainties of Planck18 (Planck Collaboration et al. 2020).

‘‘Moderate’’, and ‘‘Optimistic’’. Different foreground removal modes in 21cmSense provide estimates of the observational limits for the foreground wedge, which determines the boundary of  $k_{\parallel}$ - $k_{\perp}$  Fourier space. We show the results for moderate and optimistic removal modes in Figure 7.

At  $z = 9.4$ , the 21 cm power spectrum for  $k_{\text{trans}} = 150 \text{ Mpc}^{-1}$  is smaller than that of the fiducial model, while the power spectrum for  $k_{\text{trans}} = 400$  is larger. This is because in the  $k_{\text{trans}} = 150 \text{ Mpc}^{-1}$  model the ionizing sources are a bit more than the fiducial  $\Lambda\text{CDM}$  model, although the minihalos are also more abundant,

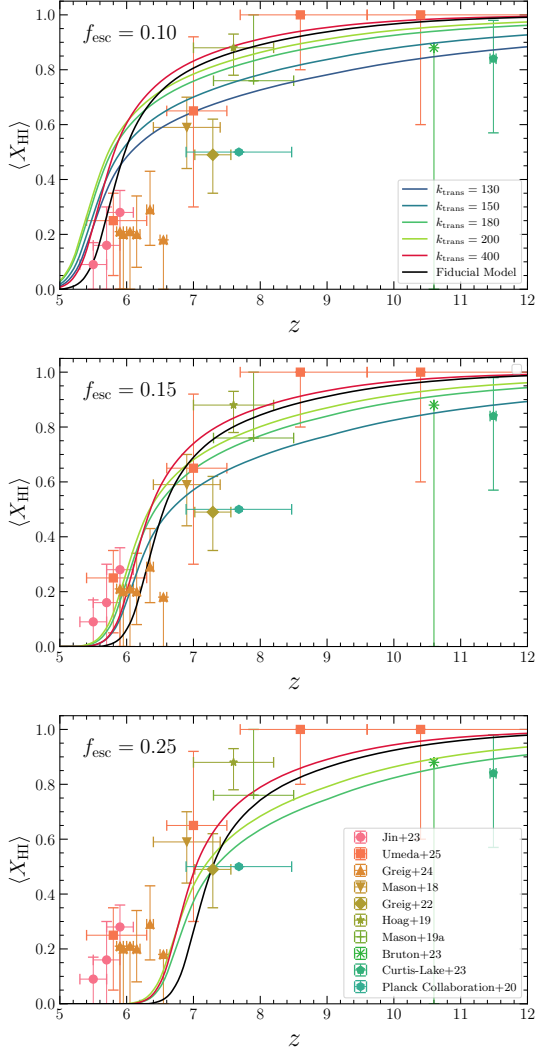


**Figure 6.** Reionization history in fiducial model and C25 models with different  $k_{\text{trans}}$  values, and in observations, including Lyman- $\alpha$  emission equivalent widths in galaxies (C. A. Mason et al. 2018, 2019; A. Hoag et al. 2019; S. Bruton et al. 2023), damping wing absorption in quasar and galaxy spectra (E. Curtis-Lake et al. 2023; B. Greig et al. 2022, 2024; H. Umeda et al. 2025), and dark pixel fractions in the Lyman- $\alpha$ /Lyman- $\beta$  forests (X. Jin et al. 2023).

the ionization is a bit promoted and the ionization fraction is a bit higher. In contrast, for the  $k_{\text{trans}} = 400 \text{ Mpc}^{-1}$  model, the ionizing sources are same to fiducial model, but minihalos consume more ionizing photons. The reionization is delayed and the ionization fraction is a bit lower, see Figure 6. The above difference in 21 cm power spectrum is larger than uncertainties of the SKA-low AA\* observations, in principle the models are distinguishable. For the  $k_{\text{trans}} = 200 \text{ Mpc}^{-1}$  model, however, the signal is very close to the fiducial model. We check that this is because in this model and at this

moment, the enhancement of ionizing photons production in halos with  $T_{\text{vir}} \gtrsim 10^4 \text{ K}$  and consumption in minihalos coincidentally counteract each other.

At  $z = 7.6$ , the difference between the fiducial model and the C25 model with  $k_{\text{trans}} = 400 \text{ Mpc}^{-1}$  becomes smaller, the  $k_{\text{trans}} = 400 \text{ Mpc}^{-1}$  model has a smaller 21 cm power spectrum at large scale ( $k \lesssim 0.3 \text{ Mpc}^{-1}$ ), but larger at small scale. However, this difference is comparable to SKA-low AA\* observational uncertainties for moderate foreground removal model, so hard to distinguish. For optimistic foreground removal model the uncertainties are smaller at larger scales  $k \lesssim 0.1 \text{ Mpc}^{-1}$ , the difference are distinguishable. The  $k_{\text{trans}} = 150 \text{ Mpc}^{-1}$  model is still a smaller than that of fiducial model, and is distinguishable. For  $k_{\text{trans}} = 200 \text{ Mpc}^{-1}$  model, the 21 cm power spectrum is lower than the fiducial model at large scale, and can be distinguished in both the moderate and optimistic foreground removal modes.

At  $z = 6.4$ , the difference between the  $k_{\text{trans}} = 400 \text{ Mpc}^{-1}$  model and the fiducial model becomes larger, the  $k_{\text{trans}} = 400 \text{ Mpc}^{-1}$  model is larger than fiducial model at  $k \gtrsim 0.06 \text{ Mpc}^{-1}$ . However the difference  $k_{\text{trans}} = 150 \text{ Mpc}^{-1}$  model and the fiducial model becomes smaller. This is because in these two models the reionization process is delayed by minihalos, see Figure 6. The difference between the three models is fully distinguishable for both the moderate and optimistic foreground removal models. For the  $k_{\text{trans}} = 200 \text{ Mpc}^{-1}$  model, at this redshift the 21 cm power spectrum is larger than the fiducial model at  $k \gtrsim 0.1 \text{ Mpc}^{-1}$ , however still smaller than the fiducial model at larger scale.

At  $z = 6.0$ , the late stage of the EoR, the 21 cm power spectra in all C25 models are larger than the fiducial model, because their reionization is delayed, and the differences are detectable for the SKA-low AA\*.

We caution that here we compare the 21 cm power spectra in different models at the same redshift. Different models have different reionization history, although the integrated  $\tau_e$  are similar. Therefore the difference in 21 cm power spectra arises from both different  $\langle X_{\text{HI}} \rangle$  and different ionized bubble morphology.

### 3.3. The bubble size distribution and detectability

In this subsection we investigate the BSD. BSD is an intuitive indicator for morphology of ionization field (S. K. Giri et al. 2018). Ionized bubbles must be identified in tomographic images, while tomographic imaging observation is far beyond the scope of SKA-low AA\*. Here we base our investigations on an assumed telescope with sensitivity much larger than the SKA-low AA\*.

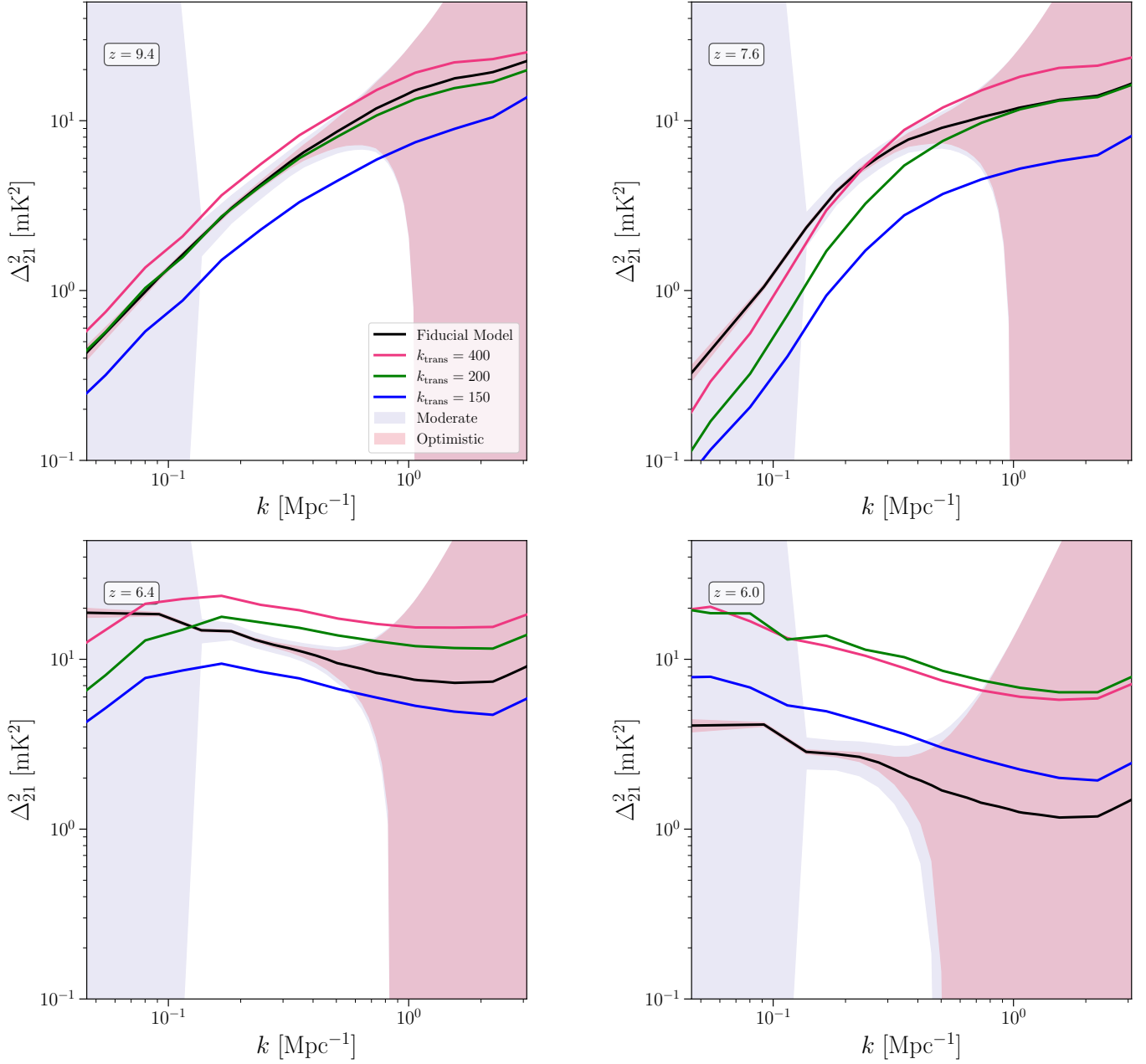


**Figure 7.** The 21 cm power spectra in fiducial model and C25 models at different redshifts and the uncertainties for SKA-low AA\* observations.

There are different methods to identify bubbles, such as distance transform (DT, [O. Zahn et al. 2007](#)), mean free path (MFP, [A. Mesinger & S. Furlanetto 2007](#)), and friends-of-friends (FoF, [I. T. Iliev et al. 2006a](#); [M. M. Friedrich et al. 2011](#)). Here we employ the MFP method provided in the code `Tools21cm` ([S. K. Giri et al. 2018](#); [S. Giri et al. 2020](#)) to derive the BSD. This method first defines the ionized region, then randomly selects an ionized point and a direction, and then records the distance to the neutral boundary along that direction. We adopt  $X_{\text{HII}} = 0.50$  as the threshold ionization fraction for ion-

ized bubbles ([A. Mesinger & S. Furlanetto 2007](#)) and construct  $10^7$  direction lines. The results for the fiducial model and C25 models are shown in left column of Figure 8, where the BSDs at stages with same  $\langle X_{\text{HII}} \rangle$  are plotted in the same panel.

We find that, in different models BSDs are rather different even for the same  $\langle X_{\text{HII}} \rangle$ . For C25 model with  $k_{\text{trans}} = 400 \text{ Mpc}^{-1}$ , the BSD is almost identical to the fiducial model at all  $\langle X_{\text{HII}} \rangle$ s. It implies that although in this model the minihalos are more abundant than fiducial model, they just globally shift the reionization

history, rather than change the morphology of ionization field. For  $k_{\text{trans}} \lesssim 400 \text{ Mpc}^{-1}$ , the BSD deviates from the fiducial model. At  $\langle X_{\text{HII}} \rangle \sim 0.25$  the peak of BSD in fiducial model is  $R \sim 8 \text{ Mpc}$ , while in  $k_{\text{trans}} = 200 \text{ Mpc}^{-1}$  and  $150 \text{ Mpc}^{-1}$  models, the peaks shift to  $R \sim 4 \text{ Mpc}$  and  $R \sim 1.3 \text{ Mpc}$  respectively. Indeed, in C25 models the ionized bubbles tend to fragment into smaller ones since minihalos intercept the propagation of ionizing photons. However, with the increasing of  $\langle X_{\text{HII}} \rangle$ , the BSDs in C25 models and in fiducial models trend to approach each others. At  $\langle X_{\text{HII}} \rangle \sim 0.75$ , almost all BSDs have peak  $R \sim 50 \text{ Mpc}$ . From this, we conclude that the best stages for detecting the small-scale enhancement of matter power spectrum is the early and mid EoR.

Ionization fields are not directly observable in practice, we also identify bubbles from mock 21 cm sky maps. To image the 21 cm fields rather than just measure the power spectrum, it requires a telescope with sensitivity much higher than SKA-low AA\*. We assume observations have angular resolution  $\sim 67''$ , frequency resolution  $\sim 0.175 \text{ MHz}$ , and noise level  $\sim 2.8 \text{ mK}$ . We add foreground from the GSM sky model (A. de Oliveira-Costa et al. 2008; H. Zheng et al. 2017) and Gaussian random noise to the 21 cm fields, to generate the mock samples. We then remove the foreground using the Singular Value Decomposition (SVD) algorithm (B. Yue et al. 2015). We adopt temperature  $0.5\langle X_{\text{HI}} \rangle$  times of the mean 21 cm brightness temperature as the threshold for bubbles, and then apply the MFP method to the foreground subtracted 21 cm sky maps. The size distributions of bubbles identified from 21 cm fields,  $\text{BSD}_{21}$ , are shown in the middle column of Figure 8. We find that for our mock samples, the influence of the foreground contamination is modest. The  $\text{BSD}_{21}$  in different models are clearly distinguishable at the early and mid EoR. However, if the noise level is much larger, then it may dominate over the bubble signal.

Since  $\delta T_b \propto (1 + \delta_b)X_{\text{HI}}$ , so the  $\text{BSD}_{21}$  derived from 21 cm fields contains not only the real ionized bubbles, but also coadjacent low-density regions miss-identified as ‘‘bubbles’’. This may attenuate the bubble information in  $\text{BSD}_{21}$ , as for both fiducial model and the C25 models, the large-scale density fields are almost the same. For this reason, we generate reference 21 cm fields by setting  $X_{\text{HI}} = 1$  everywhere, then derive  $\delta \text{BSD} = \text{BSD}_{21} - \text{BSD}_{21,\text{ref}}$ . The results are shown in the left column of Figure 8. We believe that such a quantity could be a more useful indicator for telling the morphology information of ionization fields.

## 4. SUMMARY AND DISCUSSION

### 4.1. summary

We investigated the impacts of small-scale enhanced power spectrum on reionization morphology and 21 cm signal. In such models, the number of faint galaxies and minihalos would be much more abundant than in the regular  $\Lambda\text{CDM}$  model, so the effects on reionization depends on the competition between the ionizing photons production by faint galaxies, and consumption by minihalos. However, the observed UV LFs, CMB scattering optical depth, and the reionization history exclude models with large boost on the ionizing photons production, i.e. models with  $k_{\text{trans}} \lesssim 100 - 130 \text{ Mpc}^{-1}$ .

For models with  $100 - 130 \text{ Mpc}^{-1} \lesssim k_{\text{trans}} \lesssim 400 \text{ Mpc}^{-1}$ , both the ionizing photons production in faint galaxies and consumption in minihalos are boosted, reionization process is promoted at the early EoR, but delayed at the late EoR. These effects bring us features on the 21 cm power spectrum. Compared with the fiducial model, the power spectrum is smaller at early EoR and larger at the late EoR. The differences are detectable for upcoming SKA-low AA\*. These effects also result different BSDs at the same  $\langle X_{\text{HII}} \rangle$ . The typical bubble size is obviously smaller than the fiducial model, and the difference is detectable from further telescopes that are able to do imaging observations.

For models with  $k_{\text{trans}} \gtrsim 400 \text{ Mpc}^{-1}$ , boost on ionizing photons production is negligible, therefore the impacts on reionization mainly rely on minihalos that purely consume ionizing photons, as a result the reionization process is delayed and the ionized bubbles fragment into smaller ones. The difference of the 21 cm power spectrum between such a model and fiducial model is distinguishable for the SKA-low AA\*. However, the BSD is almost the same as long as the  $\langle X_{\text{HII}} \rangle$  is the same. Therefore, combining the results of power spectrum and BSD would be useful for constraining the  $k_{\text{trans}}$  models.

### 4.2. discussion

We assume that all the minihalos must be photo-evaporated in the ionized bubbles, otherwise reionization is not able to process. This would overestimate the role played by minihalos during the EoR. Suppose the radius of the minihalo with mass  $M_{\text{mh}}$  is  $R_{\text{mh}}$  (S. R. Furlanetto & S. P. Oh 2005), then the cross-section is  $\pi R_{\text{mh}}^2$ . If the IGM is transparent to the ionizing photons and only minihalos resist them, the mean free path of an ionizing photon is

$$l_{\text{mh}} = \frac{1}{\int_{M_{\text{J}}}^{M_{\text{min}}} \pi R_{\text{mh}}^2 \frac{dn}{dm}(M_{\text{mh}}, z) dM_{\text{mh}}}. \quad (28)$$

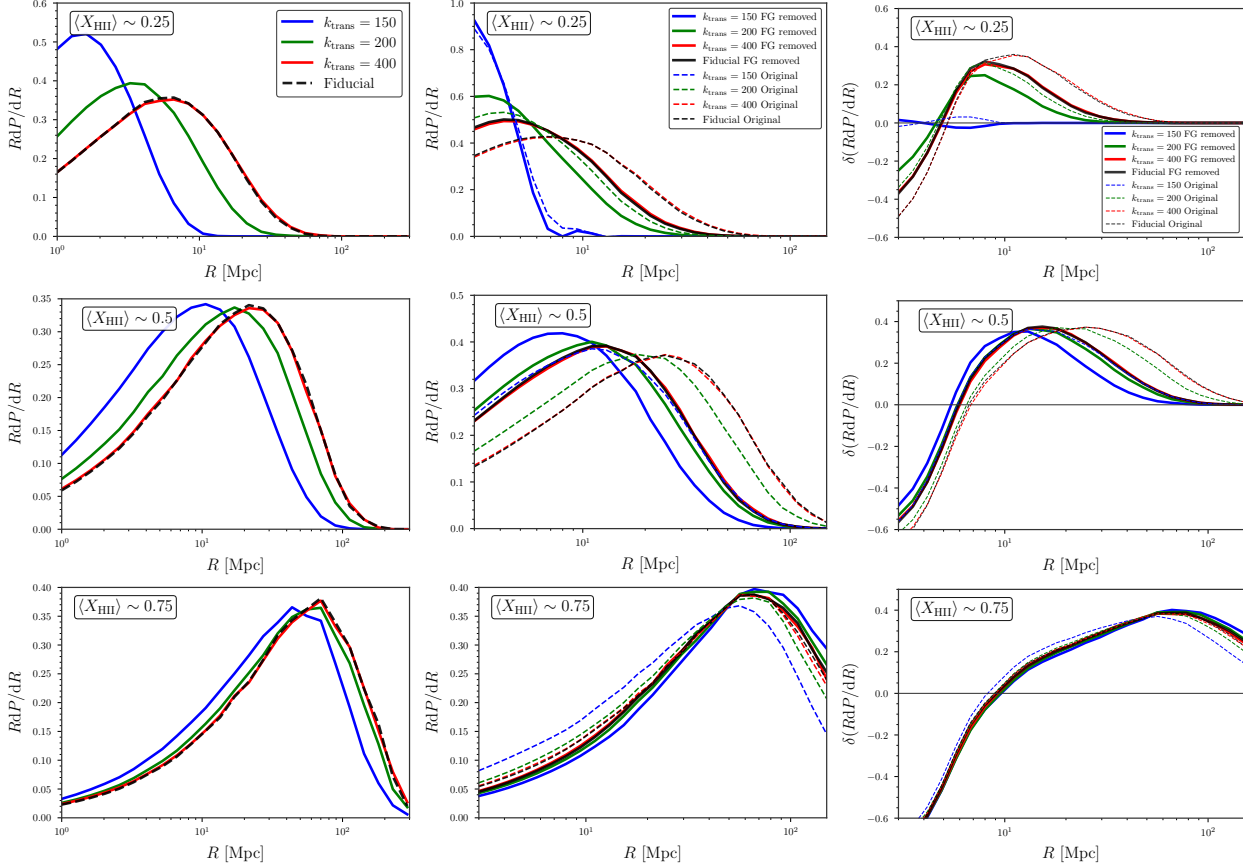


**Figure 8.** The BSD for the fiducial model and C25 models. *Top row:*  $\langle X_{\text{HII}} \rangle \sim 0.25$ . *Middle row:*  $\langle X_{\text{HII}} \rangle \sim 0.50$ . *Bottom row:*  $\langle X_{\text{HII}} \rangle \sim 0.75$ . *Left column:* the BSD is directly measured from the ionization fields. *Middle column:* the  $\text{BSD}_{21}$  is measured from the 21 cm fields, in the absence/presence of foreground contamination. *Right column:* we subtract the “BSD” of pure neutral fields from the middle column.

At  $z = 6$ , for C25 model with  $k_{\text{trans}} = 150 \text{ Mpc}^{-1}$ , the  $l_{\text{mh}} = 1.86 \text{ Mpc}$ ; for  $k_{\text{trans}} = 400 \text{ Mpc}^{-1}$ , the  $l_{\text{mh}} = 1.12 \text{ Mpc}$ ; for the fiducial model  $l_{\text{mh}} = 2.14 \text{ Mpc}$ . The fraction of ionizing photons consumed by minihalos to a distance  $R$  from a source is  $f_a = 1 - \exp(-R/l_{\text{mh}})$ . That is to say, in a spherical bubble with radius equal to 3 Mpc, the fraction of ionizing photons consumed by minihalos for these three models are 0.80, 0.93, and 0.75 respectively. According to this estimation, we believe that our assumptions should be reasonable at least for bubbles with  $R \gtrsim 3 \text{ Mpc}$ .

In our paper, we use the Jeans mass as the lower limit of minihalos that can preserve gas content. However, it has been pointed out that, filtering mass is more accurate as it accounts for the evolution history of the IGM temperature (N. Y. Gnedin & L. Hui 1998). Actually, the gas content in smaller minihalos is a complicated problem. It has been investigated by many analytical models (e.g. S. P. Oh & Z. Haiman 2003) and numerical simulations (e.g. T. K. Chan et al. 2024). They are basically consistent with each other. In T. K. Chan et al. (2024), the filtering mass is approximately 2–8 times the

Jeans mass. However, we check that if we use this filtering mass, in the C25 model with  $k_{\text{trans}} = 150 \text{ Mpc}^{-1}$ , the consumption of ionizing photons just changes negligibly. This is because in this model,  $M_{\text{h}}^{\text{bump}}$  is much larger than the Jeans mass or filtering mass, therefore most of ionizing photons are consumed in minihalos  $\gg$  the lower limit.

We always assume the matter power spectrum evolve linearly at all scales. However, at small scales the non-linear growth would be important even at redshifts as high as the EoR (I. T. Iliev et al. 2002; R. E. Smith et al. 2003; R. Takahashi et al. 2012). Generally, non-linear effect would boost the matter power spectrum and enhance the formation of minihalos. It is quite likely that if we involve this effect in our model, it will strengthen our conclusions. Moreover, there are other effects such as the dark matter - baryon relative streaming motion (e.g. S. Naoz et al. 2013) and the dark matter annihilation (e.g. E. Ripamonti et al. 2007) that may reduce the gas content of small halos and influence our conclusion. However, it is beyond the scope of this paper to investigate the explicit influence at current time.

In this work, we only consider the influence of the small-scale power spectrum enhancement on halo mass functions, ignoring the effects on the IGM. In principle, the enhancement also boosts the clumping of the IGM, so in C25 model the  $\bar{n}_{\text{rec}}$  in Eq. (19) would be larger, consuming more ionizing photons. This will further strengthen our conclusion.

Although we use the C25 model as demonstration, our methods are applicable for any power spectrum models with small-scale enhancement. Different scales and shapes of the enhancement may result in reionization histories and ionization field morphologies different from C25 model, but the conclusion – large-scale 21 cm sig-

nal statistics can reveal the enhancement, would always hold.

#### ACKNOWLEDGMENTS

We thank the anonymous referee very much for the constructive suggestions that help to improve our paper. This work is supported by the National SKA Program of China Nos. 2020SKA0110402 & 2020SKA0110401, the NSFC International (Regional) Cooperation and Exchange Project No. 12361141814, the NSFC Key Program No. 12533002, NSFC grant No. 12421003, and the Project Supported by the Specialized Research Fund for State Key Laboratory of Radio Astronomy and Technology.

#### REFERENCES

- Adamo, A., Atek, H., Bagley, M. B., et al. 2025, *Nature Astronomy*, 9, 1134, doi: [10.1038/s41550-025-02624-5](https://doi.org/10.1038/s41550-025-02624-5)
- Ali-Haïmoud, Y., Meerburg, P. D., & Yuan, S. 2014, *PhRvD*, 89, 083506, doi: [10.1103/PhysRevD.89.083506](https://doi.org/10.1103/PhysRevD.89.083506)
- Allen, B. 1985, *PhRvD*, 32, 3136, doi: [10.1103/PhysRevD.32.3136](https://doi.org/10.1103/PhysRevD.32.3136)
- Atek, H., Richard, J., Kneib, J.-P., & Schaerer, D. 2018, *MNRAS*, 479, 5184, doi: [10.1093/mnras/sty1820](https://doi.org/10.1093/mnras/sty1820)
- Atek, H., Shuntov, M., Furtak, L. J., et al. 2023, *MNRAS*, 519, 1201, doi: [10.1093/mnras/stac3144](https://doi.org/10.1093/mnras/stac3144)
- Bardeen, J. M., Bond, J. R., Kaiser, N., & Szalay, A. S. 1986, *ApJ*, 304, 15, doi: [10.1086/164143](https://doi.org/10.1086/164143)
- Barkana, R., Haiman, Z., & Ostriker, J. P. 2001, *ApJ*, 558, 482, doi: [10.1086/322393](https://doi.org/10.1086/322393)
- Barkana, R., & Loeb, A. 2001, *PhR*, 349, 125, doi: [10.1016/S0370-1573\(01\)00019-9](https://doi.org/10.1016/S0370-1573(01)00019-9)
- Barkana, R., & Loeb, A. 2002, *ApJ*, 578, 1, doi: [10.1086/342313](https://doi.org/10.1086/342313)
- Bode, P., Ostriker, J. P., & Turok, N. 2001, *ApJ*, 556, 93, doi: [10.1086/321541](https://doi.org/10.1086/321541)
- Bouwens, R. J., Illingworth, G., Ellis, R. S., Oesch, P., & Stefanon, M. 2022, *ApJ*, 940, 55, doi: [10.3847/1538-4357/ac86d1](https://doi.org/10.3847/1538-4357/ac86d1)
- Bouwens, R. J., Oesch, P. A., Illingworth, G. D., Ellis, R. S., & Stefanon, M. 2017, *ApJ*, 843, 129, doi: [10.3847/1538-4357/aa70a4](https://doi.org/10.3847/1538-4357/aa70a4)
- Bouwens, R. J., Illingworth, G. D., Oesch, P. A., et al. 2015, *ApJ*, 803, 34, doi: [10.1088/0004-637X/803/1/34](https://doi.org/10.1088/0004-637X/803/1/34)
- Bouwens, R. J., Oesch, P. A., Stefanon, M., et al. 2021, *AJ*, 162, 47, doi: [10.3847/1538-3881/abf83e](https://doi.org/10.3847/1538-3881/abf83e)
- Bouwens, R. J., Stefanon, M., Brammer, G., et al. 2023, *MNRAS*, 523, 1036, doi: [10.1093/mnras/stad1145](https://doi.org/10.1093/mnras/stad1145)
- Bowler, R. A. A., Jarvis, M. J., Dunlop, J. S., et al. 2020, *MNRAS*, 493, 2059, doi: [10.1093/mnras/staa313](https://doi.org/10.1093/mnras/staa313)
- Bradley, L. D., Coe, D., Brammer, G., et al. 2023, *ApJ*, 955, 13, doi: [10.3847/1538-4357/acecf6](https://doi.org/10.3847/1538-4357/acecf6)
- Braglia, M., Hazra, D. K., Sriramkumar, L., & Finelli, F. 2020, *JCAP*, 2020, 025, doi: [10.1088/1475-7516/2020/08/025](https://doi.org/10.1088/1475-7516/2020/08/025)
- Bruton, S., Lin, Y.-H., Scarlata, C., & Hayes, M. J. 2023, *ApJL*, 949, L40, doi: [10.3847/2041-8213/acd5d0](https://doi.org/10.3847/2041-8213/acd5d0)
- Castellano, M., Fontana, A., Treu, T., et al. 2022, *ApJL*, 938, L15, doi: [10.3847/2041-8213/ac94d0](https://doi.org/10.3847/2041-8213/ac94d0)
- Chabanier, S., Millea, M., & Palanque-Delabrouille, N. 2019, *MNRAS*, 489, 2247, doi: [10.1093/mnras/stz2310](https://doi.org/10.1093/mnras/stz2310)
- Chan, T. K., Benítez-Llambay, A., Theuns, T., Frenk, C., & Bower, R. 2024, *MNRAS*, 528, 1296, doi: [10.1093/mnras/stae114](https://doi.org/10.1093/mnras/stae114)
- Choudhury, T. R., & Chakraborty, A. 2025, *JCAP*, 2025, 114, doi: [10.1088/1475-7516/2025/10/114](https://doi.org/10.1088/1475-7516/2025/10/114)
- Choustikov, N., Stiskalek, R., Saxena, A., et al. 2025, *MNRAS*, 537, 2273, doi: [10.1093/mnras/staf126](https://doi.org/10.1093/mnras/staf126)
- Ciardi, B., Scannapieco, E., Stoehr, F., et al. 2006, *MNRAS*, 366, 689, doi: [10.1111/j.1365-2966.2005.09908.x](https://doi.org/10.1111/j.1365-2966.2005.09908.x)
- Cielo, M., Mangano, G., Pisanti, O., & Wands, D. 2025, *JCAP*, 2025, 007, doi: [10.1088/1475-7516/2025/04/007](https://doi.org/10.1088/1475-7516/2025/04/007)
- Cole, P. S., & Silk, J. 2021, *MNRAS*, 501, 2627, doi: [10.1093/mnras/staa3638](https://doi.org/10.1093/mnras/staa3638)
- Cruz, H. A. G., Muñoz, J. B., Sabti, N., & Kamionkowski, M. 2025, *PhRvD*, 111, 083503, doi: [10.1103/PhysRevD.111.083503](https://doi.org/10.1103/PhysRevD.111.083503)
- Curtis-Lake, E., Carniani, S., Cameron, A., et al. 2023, *Nature Astronomy*, 7, 622, doi: [10.1038/s41550-023-01918-w](https://doi.org/10.1038/s41550-023-01918-w)
- Dayal, P., Choudhury, T. R., Bromm, V., & Pacucci, F. 2017, *ApJ*, 836, 16, doi: [10.3847/1538-4357/836/1/16](https://doi.org/10.3847/1538-4357/836/1/16)
- Dayal, P., & Giri, S. K. 2024, *MNRAS*, 528, 2784, doi: [10.1093/mnras/stae176](https://doi.org/10.1093/mnras/stae176)

- de Oliveira-Costa, A., Tegmark, M., Gaensler, B. M., et al. 2008, *MNRAS*, 388, 247, doi: [10.1111/j.1365-2966.2008.13376.x](https://doi.org/10.1111/j.1365-2966.2008.13376.x)
- Diemand, J., Moore, B., & Stadel, J. 2005, *Nature*, 433, 389, doi: [10.1038/nature03270](https://doi.org/10.1038/nature03270)
- Donnan, C. T., McLeod, D. J., Dunlop, J. S., et al. 2023, *MNRAS*, 518, 6011, doi: [10.1093/mnras/stac3472](https://doi.org/10.1093/mnras/stac3472)
- Donnan, C. T., McLure, R. J., Dunlop, J. S., et al. 2024, *MNRAS*, 533, 3222, doi: [10.1093/mnras/stae2037](https://doi.org/10.1093/mnras/stae2037)
- Endsley, R., Behroozi, P., Stark, D. P., et al. 2020, *MNRAS*, 493, 1178, doi: [10.1093/mnras/staa324](https://doi.org/10.1093/mnras/staa324)
- Finkelstein, S. L., Ryan, Jr., R. E., Papovich, C., et al. 2015, *ApJ*, 810, 71, doi: [10.1088/0004-637X/810/1/71](https://doi.org/10.1088/0004-637X/810/1/71)
- Finkelstein, S. L., Bagley, M. B., Arrabal Haro, P., et al. 2022, *ApJL*, 940, L55, doi: [10.3847/2041-8213/ac966e](https://doi.org/10.3847/2041-8213/ac966e)
- Friedrich, M. M., Mellema, G., Alvarez, M. A., Shapiro, P. R., & Iliev, I. T. 2011, *MNRAS*, 413, 1353, doi: [10.1111/j.1365-2966.2011.18219.x](https://doi.org/10.1111/j.1365-2966.2011.18219.x)
- Furlanetto, S. R., & Oh, S. P. 2005, *MNRAS*, 363, 1031, doi: [10.1111/j.1365-2966.2005.09505.x](https://doi.org/10.1111/j.1365-2966.2005.09505.x)
- Furlanetto, S. R., Oh, S. P., & Briggs, F. H. 2006, *PhR*, 433, 181, doi: [10.1016/j.physrep.2006.08.002](https://doi.org/10.1016/j.physrep.2006.08.002)
- Furlanetto, S. R., Zaldarriaga, M., & Hernquist, L. 2004, *ApJ*, 613, 1, doi: [10.1086/423025](https://doi.org/10.1086/423025)
- Giri, S., Mellema, G., & Jensen, H. 2020, *The Journal of Open Source Software*, 5, 2363, doi: [10.21105/joss.02363](https://doi.org/10.21105/joss.02363)
- Giri, S. K., Mellema, G., Dixon, K. L., & Iliev, I. T. 2018, *MNRAS*, 473, 2949, doi: [10.1093/mnras/stx2539](https://doi.org/10.1093/mnras/stx2539)
- Gnedin, N. Y. 2016, *ApJL*, 825, L17, doi: [10.3847/2041-8205/825/2/L17](https://doi.org/10.3847/2041-8205/825/2/L17)
- Gnedin, N. Y., & Hui, L. 1998, *MNRAS*, 296, 44, doi: [10.1046/j.1365-8711.1998.01249.x](https://doi.org/10.1046/j.1365-8711.1998.01249.x)
- Gong, Y., Yue, B., Cao, Y., & Chen, X. 2023, *ApJ*, 947, 28, doi: [10.3847/1538-4357/acc109](https://doi.org/10.3847/1538-4357/acc109)
- Greig, B., Mesinger, A., Davies, F. B., et al. 2022, *MNRAS*, 512, 5390, doi: [10.1093/mnras/stac825](https://doi.org/10.1093/mnras/stac825)
- Greig, B., Mesinger, A., Bañados, E., et al. 2024, *MNRAS*, 530, 3208, doi: [10.1093/mnras/stae1080](https://doi.org/10.1093/mnras/stae1080)
- Harikane, Y., Ouchi, M., Oguri, M., et al. 2023, *ApJS*, 265, 5, doi: [10.3847/1538-4365/acaaa9](https://doi.org/10.3847/1538-4365/acaaa9)
- HERA Collaboration, Abdurashidova, Z., Adams, T., et al. 2023, *ApJ*, 945, 124, doi: [10.3847/1538-4357/acaf50](https://doi.org/10.3847/1538-4357/acaf50)
- Hirano, S., & Yoshida, N. 2024, *ApJ*, 963, 2, doi: [10.3847/1538-4357/ad22e0](https://doi.org/10.3847/1538-4357/ad22e0)
- Hoag, A., Bradač, M., Huang, K., et al. 2019, *ApJ*, 878, 12, doi: [10.3847/1538-4357/ab1de7](https://doi.org/10.3847/1538-4357/ab1de7)
- Iliev, I. T., Mellema, G., Pen, U.-L., et al. 2006a, *MNRAS*, 369, 1625, doi: [10.1111/j.1365-2966.2006.10502.x](https://doi.org/10.1111/j.1365-2966.2006.10502.x)
- Iliev, I. T., Shapiro, P. R., Ferrara, A., & Martel, H. 2002, *ApJL*, 572, L123, doi: [10.1086/341869](https://doi.org/10.1086/341869)
- Iliev, I. T., Shapiro, P. R., & Raga, A. C. 2005, *MNRAS*, 361, 405, doi: [10.1111/j.1365-2966.2005.09155.x](https://doi.org/10.1111/j.1365-2966.2005.09155.x)
- Iliev, I. T., Ciardi, B., Alvarez, M. A., et al. 2006b, *MNRAS*, 371, 1057, doi: [10.1111/j.1365-2966.2006.10775.x](https://doi.org/10.1111/j.1365-2966.2006.10775.x)
- Inman, D., & Kohri, K. 2023, *PhRvD*, 107, 123513, doi: [10.1103/PhysRevD.107.123513](https://doi.org/10.1103/PhysRevD.107.123513)
- Iršič, V., Viel, M., Haehnelt, M. G., et al. 2017, *PhRvD*, 96, 023522, doi: [10.1103/PhysRevD.96.023522](https://doi.org/10.1103/PhysRevD.96.023522)
- Ishigaki, M., Kawamata, R., Ouchi, M., et al. 2018, *ApJ*, 854, 73, doi: [10.3847/1538-4357/aaa544](https://doi.org/10.3847/1538-4357/aaa544)
- Jenkins, A., Frenk, C. S., White, S. D. M., et al. 2001, *MNRAS*, 321, 372, doi: [10.1046/j.1365-8711.2001.04029.x](https://doi.org/10.1046/j.1365-8711.2001.04029.x)
- Jin, X., Yang, J., Fan, X., et al. 2023, *ApJ*, 942, 59, doi: [10.3847/1538-4357/aca678](https://doi.org/10.3847/1538-4357/aca678)
- Jones, D., Palatnick, S., Chen, R., Beane, A., & Lidz, A. 2021, *ApJ*, 913, 7, doi: [10.3847/1538-4357/abf0a9](https://doi.org/10.3847/1538-4357/abf0a9)
- Klessen, R. S., & Glover, S. C. O. 2023, *ARA&A*, 61, 65, doi: [10.1146/annurev-astro-071221-053453](https://doi.org/10.1146/annurev-astro-071221-053453)
- Koprowski, M. P., Coppin, K. E. K., Geach, J. E., et al. 2018, *MNRAS*, 479, 4355, doi: [10.1093/mnras/sty1527](https://doi.org/10.1093/mnras/sty1527)
- Kroupa, P. 2001, *MNRAS*, 322, 231, doi: [10.1046/j.1365-8711.2001.04022.x](https://doi.org/10.1046/j.1365-8711.2001.04022.x)
- Lazare, H., Flitter, J., & Kovetz, E. D. 2024, *PhRvD*, 110, 123532, doi: [10.1103/PhysRevD.110.123532](https://doi.org/10.1103/PhysRevD.110.123532)
- Leitherer, C., & Chen, J. 2009, *NewA*, 14, 356, doi: [10.1016/j.newast.2008.10.007](https://doi.org/10.1016/j.newast.2008.10.007)
- Leitherer, C., Ekström, S., Meynet, G., et al. 2014, *ApJS*, 212, 14, doi: [10.1088/0067-0049/212/1/14](https://doi.org/10.1088/0067-0049/212/1/14)
- Leitherer, C., Schaerer, D., Goldader, J. D., et al. 1999, *ApJS*, 123, 3, doi: [10.1086/313233](https://doi.org/10.1086/313233)
- Lewis, A., Challinor, A., & Lasenby, A. 2000, *ApJ*, 538, 473, doi: [10.1086/309179](https://doi.org/10.1086/309179)
- Liu, B., Shan, H., & Zhang, J. 2024, *ApJ*, 968, 79, doi: [10.3847/1538-4357/ad4ed8](https://doi.org/10.3847/1538-4357/ad4ed8)
- Liu, S., Liu, Y., Peng, B., et al. 2025, arXiv e-prints, arXiv:2508.10176, doi: [10.48550/arXiv.2508.10176](https://doi.org/10.48550/arXiv.2508.10176)
- Livermore, R. C., Finkelstein, S. L., & Lotz, J. M. 2017, *ApJ*, 835, 113, doi: [10.3847/1538-4357/835/2/113](https://doi.org/10.3847/1538-4357/835/2/113)
- Loeb, A., & Zaldarriaga, M. 2004, *PhRvL*, 92, 211301, doi: [10.1103/PhysRevLett.92.211301](https://doi.org/10.1103/PhysRevLett.92.211301)
- Mao, Y., Koda, J., Shapiro, P. R., et al. 2020, *MNRAS*, 491, 1600, doi: [10.1093/mnras/stz2986](https://doi.org/10.1093/mnras/stz2986)
- Mason, C. A., Treu, T., Dijkstra, M., et al. 2018, *ApJ*, 856, 2, doi: [10.3847/1538-4357/aab0a7](https://doi.org/10.3847/1538-4357/aab0a7)
- Mason, C. A., Fontana, A., Treu, T., et al. 2019, *MNRAS*, 485, 3947, doi: [10.1093/mnras/stz632](https://doi.org/10.1093/mnras/stz632)
- McBride, J., Fakhouri, O., & Ma, C.-P. 2009, *MNRAS*, 398, 1858, doi: [10.1111/j.1365-2966.2009.15329.x](https://doi.org/10.1111/j.1365-2966.2009.15329.x)

- McLure, R. J., Dunlop, J. S., Bowler, R. A. A., et al. 2013, *MNRAS*, 432, 2696, doi: [10.1093/mnras/stt627](https://doi.org/10.1093/mnras/stt627)
- Mesinger, A., & Furlanetto, S. 2007, *ApJ*, 669, 663, doi: [10.1086/521806](https://doi.org/10.1086/521806)
- Mesinger, A., Furlanetto, S., & Cen, R. 2011, *MNRAS*, 411, 955, doi: [10.1111/j.1365-2966.2010.17731.x](https://doi.org/10.1111/j.1365-2966.2010.17731.x)
- Mo, H. J., & White, S. D. M. 1996, *MNRAS*, 282, 347, doi: [10.1093/mnras/282.2.347](https://doi.org/10.1093/mnras/282.2.347)
- Muñoz, J. B., Dvorkin, C., & Cyr-Racine, F.-Y. 2020, *PhRvD*, 101, 063526, doi: [10.1103/PhysRevD.101.063526](https://doi.org/10.1103/PhysRevD.101.063526)
- Murray, S., Greig, B., Mesinger, A., et al. 2020, *The Journal of Open Source Software*, 5, 2582, doi: [10.21105/joss.02582](https://doi.org/10.21105/joss.02582)
- Murray, S. G., Pober, J., & Kolopanis, M. 2024, *Journal of Open Source Software*, 9, 6501, doi: [10.21105/joss.06501](https://doi.org/10.21105/joss.06501)
- Nadler, E. O., Gluscevic, V., & Benson, A. 2025, *ApJ*, 993, 17, doi: [10.3847/1538-4357/ae073b](https://doi.org/10.3847/1538-4357/ae073b)
- Naidu, R. P., Oesch, P. A., van Dokkum, P., et al. 2022, *ApJL*, 940, L14, doi: [10.3847/2041-8213/ac9b22](https://doi.org/10.3847/2041-8213/ac9b22)
- Naoz, S., Yoshida, N., & Gnedin, N. Y. 2013, *ApJ*, 763, 27, doi: [10.1088/0004-637X/763/1/27](https://doi.org/10.1088/0004-637X/763/1/27)
- Ocvirk, P., Aubert, D., Sorce, J. G., et al. 2020, *MNRAS*, 496, 4087, doi: [10.1093/mnras/staa1266](https://doi.org/10.1093/mnras/staa1266)
- Oh, S. P., & Haiman, Z. 2003, *MNRAS*, 346, 456, doi: [10.1046/j.1365-2966.2003.07103.x](https://doi.org/10.1046/j.1365-2966.2003.07103.x)
- Park, J., Mesinger, A., Greig, B., & Gillet, N. 2019, *MNRAS*, 484, 933, doi: [10.1093/mnras/stz032](https://doi.org/10.1093/mnras/stz032)
- Planck Collaboration, Aghanim, N., Akrami, Y., et al. 2020, *A&A*, 641, A6, doi: [10.1051/0004-6361/201833910](https://doi.org/10.1051/0004-6361/201833910)
- Poher, J. C., Parsons, A. R., DeBoer, D. R., et al. 2013, *AJ*, 145, 65, doi: [10.1088/0004-6256/145/3/65](https://doi.org/10.1088/0004-6256/145/3/65)
- Poher, J. C., Liu, A., Dillon, J. S., et al. 2014, *ApJ*, 782, 66, doi: [10.1088/0004-637X/782/2/66](https://doi.org/10.1088/0004-637X/782/2/66)
- Pritchard, J. R., & Loeb, A. 2012, *Reports on Progress in Physics*, 75, 086901, doi: [10.1088/0034-4885/75/8/086901](https://doi.org/10.1088/0034-4885/75/8/086901)
- Ripamonti, E., Mapelli, M., & Ferrara, A. 2007, *MNRAS*, 375, 1399, doi: [10.1111/j.1365-2966.2006.11402.x](https://doi.org/10.1111/j.1365-2966.2006.11402.x)
- Rudakovskiy, A., Mesinger, A., Savchenko, D., & Gillet, N. 2021, *MNRAS*, 507, 3046, doi: [10.1093/mnras/stab2333](https://doi.org/10.1093/mnras/stab2333)
- Shao, Y., Xu, Y., Wang, Y., et al. 2023, *Nature Astronomy*, 7, 1116, doi: [10.1038/s41550-023-02024-7](https://doi.org/10.1038/s41550-023-02024-7)
- Shapiro, P. R., Iliev, I. T., & Raga, A. C. 2004, *MNRAS*, 348, 753, doi: [10.1111/j.1365-2966.2004.07364.x](https://doi.org/10.1111/j.1365-2966.2004.07364.x)
- Sheth, R. K., & Tormen, G. 1999, *MNRAS*, 308, 119, doi: [10.1046/j.1365-8711.1999.02692.x](https://doi.org/10.1046/j.1365-8711.1999.02692.x)
- Shimabukuro, H., Ichiki, K., & Kadota, K. 2020a, *PhRvD*, 101, 043516, doi: [10.1103/PhysRevD.101.043516](https://doi.org/10.1103/PhysRevD.101.043516)
- Shimabukuro, H., Ichiki, K., & Kadota, K. 2020b, *PhRvD*, 102, 023522, doi: [10.1103/PhysRevD.102.023522](https://doi.org/10.1103/PhysRevD.102.023522)
- Shull, J. M., France, K., Danforth, C. W., Smith, B., & Tumlinson, J. 2010, *ApJ*, 722, 1312, doi: [10.1088/0004-637X/722/2/1312](https://doi.org/10.1088/0004-637X/722/2/1312)
- Shull, J. M., Harness, A., Trenti, M., & Smith, B. D. 2012, *ApJ*, 747, 100, doi: [10.1088/0004-637X/747/2/100](https://doi.org/10.1088/0004-637X/747/2/100)
- Sikder, S., Park, H., Barkana, R., Yoshida, N., & Fialkov, A. 2025, *arXiv e-prints*, arXiv:2509.11175, doi: [10.48550/arXiv.2509.11175](https://doi.org/10.48550/arXiv.2509.11175)
- Sipple, J., Lidz, A., Grin, D., & Sun, G. 2025, *MNRAS*, 538, 1830, doi: [10.1093/mnras/staf340](https://doi.org/10.1093/mnras/staf340)
- Smith, R. E., & Markovic, K. 2011, *PhRvD*, 84, 063507, doi: [10.1103/PhysRevD.84.063507](https://doi.org/10.1103/PhysRevD.84.063507)
- Smith, R. E., Peacock, J. A., Jenkins, A., et al. 2003, *MNRAS*, 341, 1311, doi: [10.1046/j.1365-8711.2003.06503.x](https://doi.org/10.1046/j.1365-8711.2003.06503.x)
- Tacchella, S., Bose, S., Conroy, C., Eisenstein, D. J., & Johnson, B. D. 2018, *ApJ*, 868, 92, doi: [10.3847/1538-4357/aae8e0](https://doi.org/10.3847/1538-4357/aae8e0)
- Takahashi, R., Sato, M., Nishimichi, T., Taruya, A., & Oguri, M. 2012, *ApJ*, 761, 152, doi: [10.1088/0004-637X/761/2/152](https://doi.org/10.1088/0004-637X/761/2/152)
- Tkachev, M. V., Pilipenko, S. V., Mikheeva, E. V., & Lukash, V. N. 2024, *MNRAS*, 527, 1381, doi: [10.1093/mnras/stad3279](https://doi.org/10.1093/mnras/stad3279)
- Umeda, H., Ouchi, M., Kageura, Y., et al. 2025, *arXiv e-prints*, arXiv:2504.04683, doi: [10.48550/arXiv.2504.04683](https://doi.org/10.48550/arXiv.2504.04683)
- Vázquez, G. A., & Leitherer, C. 2005, *ApJ*, 621, 695, doi: [10.1086/427866](https://doi.org/10.1086/427866)
- Viel, M., Becker, G. D., Bolton, J. S., & Haehnelt, M. G. 2013, *PhRvD*, 88, 043502, doi: [10.1103/PhysRevD.88.043502](https://doi.org/10.1103/PhysRevD.88.043502)
- Viel, M., Lesgourgues, J., Haehnelt, M. G., Matarrese, S., & Riotto, A. 2005, *PhRvD*, 71, 063534, doi: [10.1103/PhysRevD.71.063534](https://doi.org/10.1103/PhysRevD.71.063534)
- Villasenor, B., Robertson, B., Madau, P., & Schneider, E. 2023, *PhRvD*, 108, 023502, doi: [10.1103/PhysRevD.108.023502](https://doi.org/10.1103/PhysRevD.108.023502)
- Vogelsberger, M., McKinnon, R., O'Neil, S., et al. 2019, *MNRAS*, 487, 4870, doi: [10.1093/mnras/stz1644](https://doi.org/10.1093/mnras/stz1644)
- Wang, J., Bose, S., Frenk, C. S., et al. 2020, *Nature*, 585, 39, doi: [10.1038/s41586-020-2642-9](https://doi.org/10.1038/s41586-020-2642-9)
- Weisz, D. R., Johnson, B. D., & Conroy, C. 2014, *ApJL*, 794, L3, doi: [10.1088/2041-8205/794/1/L3](https://doi.org/10.1088/2041-8205/794/1/L3)
- Witstok, J., Jakobsen, P., Maiolino, R., et al. 2025, *Nature*, 639, 897, doi: [10.1038/s41586-025-08779-5](https://doi.org/10.1038/s41586-025-08779-5)
- Wu, Z., & Kravtsov, A. 2024, *The Open Journal of Astrophysics*, 7, 56, doi: [10.33232/001c.121193](https://doi.org/10.33232/001c.121193)
- Yue, B., & Chen, X. 2012, *ApJ*, 747, 127, doi: [10.1088/0004-637X/747/2/127](https://doi.org/10.1088/0004-637X/747/2/127)

- Yue, B., Ciardi, B., Scannapieco, E., & Chen, X. 2009, MNRAS, 398, 2122, doi: [10.1111/j.1365-2966.2009.15261.x](https://doi.org/10.1111/j.1365-2966.2009.15261.x)
- Yue, B., Ferrara, A., Pallottini, A., Gallerani, S., & Vallini, L. 2015, MNRAS, 450, 3829, doi: [10.1093/mnras/stv933](https://doi.org/10.1093/mnras/stv933)
- Yue, B., Ferrara, A., & Xu, Y. 2016, MNRAS, 463, 1968, doi: [10.1093/mnras/stw2145](https://doi.org/10.1093/mnras/stw2145)
- Yue, B., Castellano, M., Ferrara, A., et al. 2018, ApJ, 868, 115, doi: [10.3847/1538-4357/aae77f](https://doi.org/10.3847/1538-4357/aae77f)
- Yung, L. Y. A., Somerville, R. S., Finkelstein, S. L., Popping, G., & Davé, R. 2019, MNRAS, 483, 2983, doi: [10.1093/mnras/sty3241](https://doi.org/10.1093/mnras/sty3241)
- Zahn, O., Lidz, A., McQuinn, M., et al. 2007, ApJ, 654, 12, doi: [10.1086/509597](https://doi.org/10.1086/509597)
- Zel'dovich, Y. B. 1970, A&A, 5, 84
- Zhang, M., Yue, B., Xu, Y., & Ferrara, A. 2025, ApJ, 984, 100, doi: [10.3847/1538-4357/adc730](https://doi.org/10.3847/1538-4357/adc730)
- Zhang, X., Yue, B., Shi, Y., Wu, F., & Chen, X. 2023, ApJ, 945, 109, doi: [10.3847/1538-4357/acb6fe](https://doi.org/10.3847/1538-4357/acb6fe)
- Zheng, H., Tegmark, M., Dillon, J. S., et al. 2017, MNRAS, 464, 3486, doi: [10.1093/mnras/stw2525](https://doi.org/10.1093/mnras/stw2525)